Research Square

Preprints are preliminary reports that have not undergone peer review.
They should not be considered conclusive, used to inform clinical practice,
or referenced by the media as validated information.

# Long term temperature monitoring, regime shift detection, and machine learning–based seasonal forecast in the mountainous region of northeast India

**Goutam Elangbam**
Manipur University
**Abujam Manglem Singh**
amanglem@yahoo.com

Manipur University https://orcid.org/0000-0002-3546-3617

**Research Article**

**Keywords:** Manipur, temperature trends, ERA5, Modified Mann–Kendall, machine learning forecasting

**Posted Date:** June 11th, 2026

**DOI:** https://doi.org/10.21203/rs.3.rs-9813836/v1

**License:** This work is licensed under a Creative Commons Attribution 4.0 International License.
Read Full License

**Version of Record:** A version of this preprint was published at Acta Geophysica on September 3rd, 2026.
See the published version at https://doi.org/10.1007/s11600-026-01996-0.

# Long term temperature monitoring, regime shift detection, and machine learning–based seasonal forecast in the mountainous region of northeast India

**1. Goutam Elangbam**

Department of Geography, Manipur University

Canchipur, Imphal-795003, Manipur, India

City: Imphal

Email: gtmelangba@gmail.com

ORCID: 0009-0004-0443-0347

**2. Abujam Manglem Singh ***

Department of Geography, Manipur University

Canchipur, Imphal-795003, Manipur, India

City: Imphal

Email: amanglem@yahoo.com

ORCID: 0000-0002-3546-3617

*Corresponding author: Abujam Manglem Singh

## Declarations

**Author Contributions:**

All authors contributed equally

**Funding**

No funding was obtained for this study

**Ethics approval and Consent to Participate**

Not applicable

**Competing Interest**

No competing interest

**Consent to Publication**

Author approved the manuscript

**Conflict of Interest**

No conflict of interest

**Data Availability Statement**

The dataset generated during and /or analysed during the current study are available from the corresponding author upon reasonable request

# Long term temperature monitoring, regime shift detection, and machine learning–based seasonal forecast in the mountainous region of northeast India


## Abstract

Monitoring long-term temperature variability and near-term temperature projections is essential for evidence-based climate adaptation planning in data-sparse, climate-sensitive mountainous regions. In this context, the present study integrated historical temperature trends, abrupt regime shifts, spatiotemporal warming patterns, and machine-learning–based seasonal forecasts in Manipur, a hilly state in Northeast India. The analysis was based on validated high-resolution ERA5 reanalysis data (0.25° × 0.25°) spanning 1940–2021 across 33 grid points. For statistical and spatial change mapping, the Modified Mann–Kendall test, Sen's slope estimator, Pettitt's test and spatial interpolation techniques were used. Results revealed statistically significant increasing trends in annual minimum (Tmin), maximum (Tmax), and mean (Tmean) temperatures, with warming rates 0.016°C/yr, 0.020°C/yr, and 0.017°C/yr, respectively. Abrupt change points were detected at 1985 (Tmin), 1992 (Tmax), and 1984 (Tmean), suggesting a transition to a warming phase concentrated in the mid-1980s to early 1990s. However, warming was spatially uneven, with the western and southwestern areas experiencing the most pronounced warming while the northeastern parts registering comparatively lower rates of increase. Seasonal temperature forecasts for 2022–2030, generated using Support Vector Regression (SVR) and Artificial Neural Network–Multi-Layer Perceptron (ANN-MLP) models, projected continued warming, particularly during the summer and post-monsoon seasons. Although inter-model divergence was observed in winter Tmin forecasts, SVR generally performed better than ANN-MLP for Tmin and Tmean across most seasons. The study highlighted the effectiveness of integrating statistical trend analysis and machine-learning approaches for historical and future temperature forecasting to inform climate resilience planning. Moreover, the it also offers a replicable framework for similar investigations in mountainous regions of the wider tropics.



Keywords: Manipur; temperature trends; ERA5; Modified Mann–Kendall; machine learning forecasting.

## INTRODUCTION

Climate change is widely recognised as one of the most pressing global environmental challenges, manifested through persistent increases in temperature, shifts in climatic regimes, and a rising frequency of extreme weather events (IPCC 2021). Warming has accelerated markedly over the past century, driven primarily by increasing greenhouse gas concentrations, leading to widespread alterations in the Earth's climate system (Hansen et al. 2025). The latest report on the State of the Global Climate confirms that 2015-2025 were the hottest 11 years on record, with the annually averaged global mean near-surface temperature in 2025 being 1.43 °C ± 0.13 °C above the industrial-era average (WMO 2026). The report further documents warming's profound influence on hydrological systems, ecosystems, agriculture, and human well-being across diverse geographical contexts. In recent decades, mountain regions have experienced greater warming than other terrain types (Pepin et al. 2025). Increased atmospheric moisture at high elevations, leading to enhanced downward longwave radiation, has been identified as the key physical driver of elevation-dependent warming in mountainous terrain (Palazzi et al. 2018; Rangwala et al. 2013).

Indian subcontinent has experienced substantial warming over recent decades, characterised by significant increases in annual and seasonal temperatures, a narrowing diurnal temperature range, and intensified heatwaves (Banerjee et al. 2025). The Himalaya region has become hotspot of climate change with system wide documented alterations in its climate affecting ecosystem services that benefit millions of people (Chauhan et al.2023). Within this broader national context, Northeast India, being part of the Himalayas, has registered rapid warming relative to surrounding lowlands, reflecting the combined influence of complex topography, monsoonal circulation, and land–atmosphere interactions (Krishnan et al. 2020). This pattern of warming is a characteristic of the wider tropical mountainous regions of the world. The region is also a climate-sensitive region owing to its strong monsoonal influence and highly complex terrain. Studies have documented increased minimum and mean temperatures, and elevation-linked variability across the region (Kumar et al. 2020; Ahamed et al. 2024). Singh et al. (2021) identified persistent long-term climatic shifts, including temperature-induced hydroclimatic changes in the region and the eastern Himalayan extension, while Manzoor and Ahanger (2022) reported a region-wide warming in the Himalayan states of India. Gautam et al.'s (2025) study further confirmed statistically significant warming trends and shifts in temperature regimes, indicating persistent and accelerating warming signals in the region. The documented warming across Northeast India and its adjoining regions is expected to exert profound impacts on regional biodiversity and increase climate-related vulnerabilities in hydrological systems, agriculture, ecosystems, and human settlements.

The warming across the region till date has been predominantly identified through analyses of long-term observational and gridded datasets (interpolated from observed and reanalysis data) focusing on evaluating historical temperature changes (Gautam et al. 2025). However, to develop informed mitigation and adaptation policies to reduce and avoid future impacts from persistent warming, there is a strong need to understand the patterns of future temperature behaviour, in addition to historical examinations. At present, few studies have attempted to project future temperature conditions in Northeast India. Existing projection studies have largely relied on general circulation model (GCM)–based approaches. For instance, Paul and Maity (2023) employed CMIP6 projections to estimate substantial future increases in maximum and minimum temperatures across Northeast India under high-emission scenarios. In contrast, Rahman and Pekkat (2025) used machine-learning–

driven multi-model ensemble approaches applied to long-term temperature observations, which can substantially improve the prediction of maximum and minimum temperatures across the region.

On the other hand, the data-driven, flexible nature of machine-learning (ML) techniques has shown a clear advantage over traditional statistical and dynamical approaches for predicting climate variables, particularly under changing climatic conditions. Machine-learning models can learn complex, nonlinear relationships directly from historical climate data without requiring explicit physical parameterisation (Saha et al. 2020). Consequently, temperature prediction studies have employed a wide range of ML techniques (Shrivastava et al. 2023), which can be broadly categorized into traditional statistical and machine-learning methods (e.g., regression, support vector machines, and tree-based ensemble models), artificial neural networks (ANN) such as multi-layer perceptron (MLP) for modelling nonlinear relationships, and more advanced deep-learning architectures, including convolutional neural networks (CNNs), long short-term memory networks (LSTMs), and hybrid spatio-temporal models capable of capturing complex spatial and temporal dependencies in high-dimensional climate data (Kent et al. 2025; Alkhezi 2026). Despite recent methodological developments, the application of such approaches to long-term temperature assessment and near-term seasonal forecasting in topographically complex, data-sparse mountain regions of Northeast India remains critically underexplored.

Another issue with the existing literature on temperature analysis for the region is that previous studies have been geographically uneven in coverage and methodologically incomplete. For instance, regional-scale assessments by Gautam et al. (2025) provide broad warming signals but lack the state-level resolution needed for localised adaptation planning. Available studies at this scale are limited to Assam (Tamuly et al. 2019; Ahmed et al. 2022) and, to a lesser extent, to Meghalaya (Saha et al. 2025). The interior hill states, including Nagaland, Mizoram and Manipur, have remained almost entirely unexamined at this level (Roy et al. 2021; Pandey et al. 2024).

This study, therefore, provides a case for providing an integrated assessment combining long-term temperature analysis for spatiotemporal characterization, and ML-based seasonal forecasting specifically in Manipur. The state's complex topography, a severely sparse observational network, and high socio-ecological climate sensitivity broadly represent the conditions of India's northeast and tropical mountainous regions. Therefore, the framework and findings from the study may offer a replicable analytical framework for analogous data-scarce states across the broader eastern Himalayan region and wider monsoon tropics. Specifically, the present study examines long-term temperature variability in Manipur using high-resolution ERA5 reanalysis data (1940–2021), integrating nonparametric trend analysis, regime-shift detection, spatiotemporal characterization, and ML-based seasonal forecasting within a single coherent analytical framework.

The specific objectives of this study are to: (i) examine changing patterns of temperature fluctuation and variability, (ii) detect long-term trends and abrupt change points, (iii) visualise spatial and temporal warming patterns, and (iv) forecast near-term seasonal temperatures of Manipur. To achieve these objectives, nonparametric statistical techniques for trend and change-point detection, Inverse Distance Weighted interpolation for spatiotemporal characterization, and Support Vector Regression (SVR) and Artificial Neural Network–Multi-Layer Perceptron (ANN-MLP) models for seasonal temperature forecasting are employed.

## METHODOLOGY

### Study Area

Manipur, situated in northeastern India, covers an area of approximately 22,327 km². The state lies between 92°58′23.422″ E and 94°43′35.553″ E longitudes and 23°49′45.530″ N and 25°42′1.456″ N latitudes (Fig. 1). Physiographically, rugged hilly terrain occupies about 90% of the geographical area, while the saucer-shaped Imphal Valley constitutes the remaining 10%. The state's altitude ranges from 8 m in the valley to 2,984 m, with multiple parallel hill ranges running NNE to SSW—northern hills reaching 2,000–3,000 m, while southern hills are lower (800–1,500 m). The state has a humid subtropical monsoonal climate (Cwa) according to the Köppen-Geiger classification (Beck et al. 2018). The summer season (March to May) is hot, with temperatures reaching up to 35–38°C, though they usually drop after frequent thunderstorm showers. The monsoon months (June to September) are warm (25–32°C) but cooler than summer, due to heavy rainfall (1,200–2,700 mm annually). In contrast, the winter season (December to February) is cold and dry with temperatures ranging between 5–20°C. Annual mean temperatures span 14.5–25°C spatially, driven by elevation. The state is ecologically part of the environmentally fragile eastern Indian Himalayan Region (IHR), a region deemed one of the most climate-vulnerable regions of South Asia (Elangbam and Singh 2025; Sekhri et al. 2020). Changes in temperature and monsoon rainfall patterns in Manipur have already placed critical sectors, including agriculture, water resources, forestry, and public health, under increasing stress (Sharma et al. 2024). This vulnerability is further intensified by the strong dependence of the state's majority population, i.e. low-income communities, on climate-sensitive agriculture and allied activities for their livelihoods. Future changes in these climatic variables are likely to place additional pressure on regional ecosystems, thereby further threatening livelihood security and socio-ecological sustainability across the state. As such, evaluating historical temperature variability and providing reliable information on future temperature changes are imperative for guiding adaptation planning and management strategies across ecosystems, water resources, agriculture, and other climate-sensitive sectors.

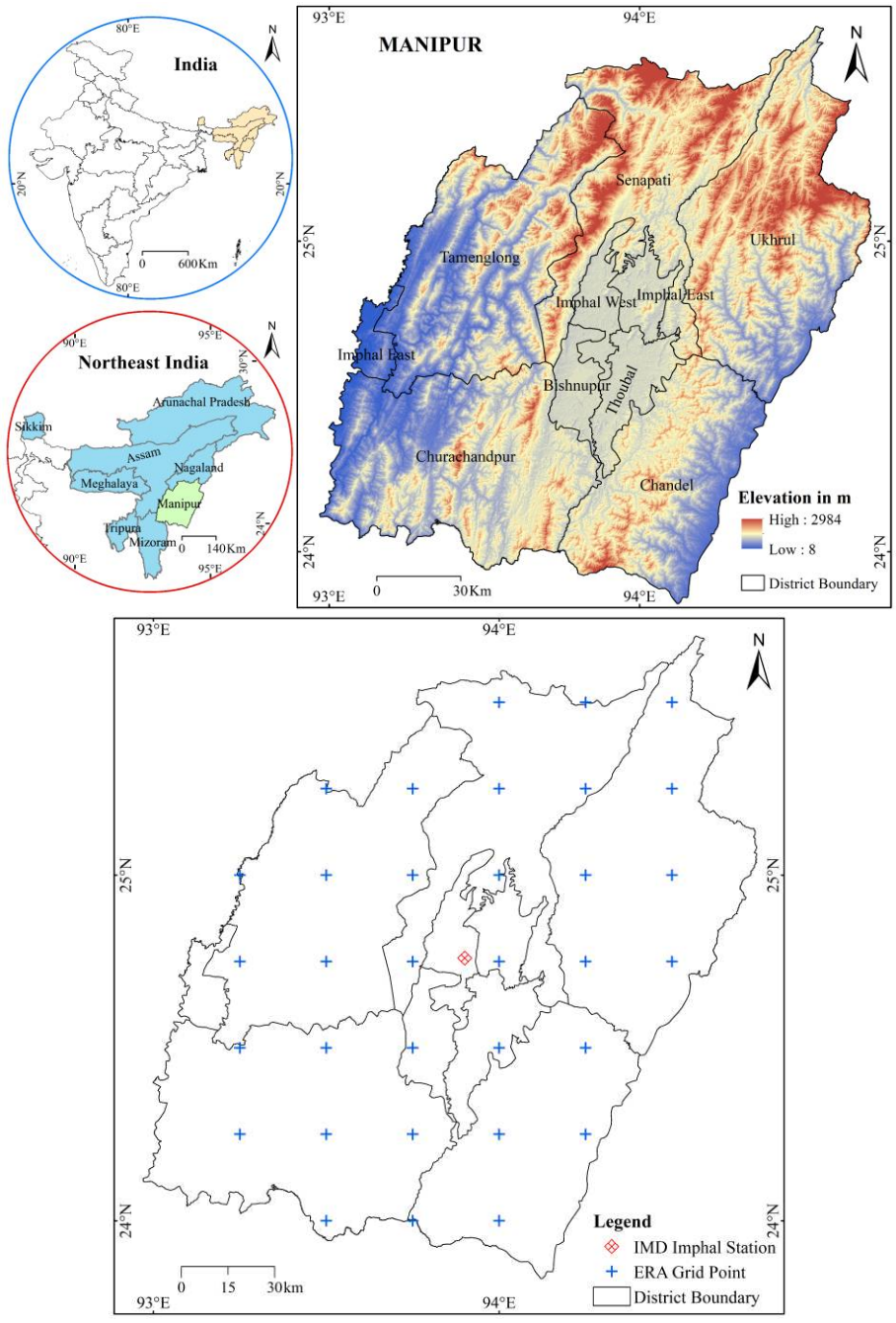



**Fig. 1** Location map of the study area showing Manipur state boundary, ERA5 reanalysis grid points (n=33, 0.25° × 0.25° resolution), and the IMD surface meteorological station at Imphal (24°46'N, 93°54'E).

## Data

This study uses temperature data from the European Centre for Medium-Range Weather Forecasts Reanalysis 5th Generation (ERA5). The ERA5 dataset has a spatial resolution of 0.25° × 0.25° and covers the period from 1940 to the present. For this study, temperature data were extracted from 33 grid points located within the study area for the period 1940–2021. Previous studies have shown that ERA5 data perform well in representing observed temperature patterns in many parts of the world, including India (Liu et al. 2024; Vishal and Rani 2022). However, validation with observed data is necessary, especially in regions with low station density, such as Northeast India

(Satyapragyan et al. 2026). Therefore, the accuracy of the ERA5 data was assessed using station data from the study area, performed by comparing the minimum temperature (Tmin), maximum temperature (Tmax), and mean temperature (Tmean) data of the ERA5 grid point (24.75°N, 93.75°E) located nearest to the Indian Meteorological Department (IMD) station (Imphal; 24°46′N, 93°54′E; elevation 781 m above sea level) over the period from 1969 to 2018, which included a total of 600 observations. The statistical measures, including the Pearson correlation coefficient (r), bias (ERA5 minus IMD), root mean square error (RMSE), and mean absolute error (MAE), were calculated for the purpose of evaluating the performance of ERA5 data. ERA5 validation against IMD Imphal station data (1969–2018, n=600) shows strong agreement ($r > 0.95$ for Tmin, Tmax, Tmean), low RMSE, and consistent biases typical of reanalyses in complex terrain (Fig.2). However, in sparse regions like Northeast India's hills, ERA5 may overestimate warming due to limited gauge input and elevation effects, as noted in validation studies (e.g., positive Tmin bias in mountains). Trends here focus on relative changes, robust to such biases. Moreover, the suitability of ERA5 for long-term trend analysis is established because relative changes over time rather than absolute values are the primary analytical focus in this study. After validating the ERA5 data, autocorrelation was evaluated to determine whether the Modified Mann–Kendall (MMK) test should be applied instead of the classical Mann-Kendall (MK) test. Autocorrelation functions (ACFs) were calculated up to lag 19, and Durbin–Watson (DW) statistics were computed for temperature variables ($T_{min}$, $T_{max,}$ and $T_{mean}$). Figure 3 illustrates the detail methodology adopted in the study.

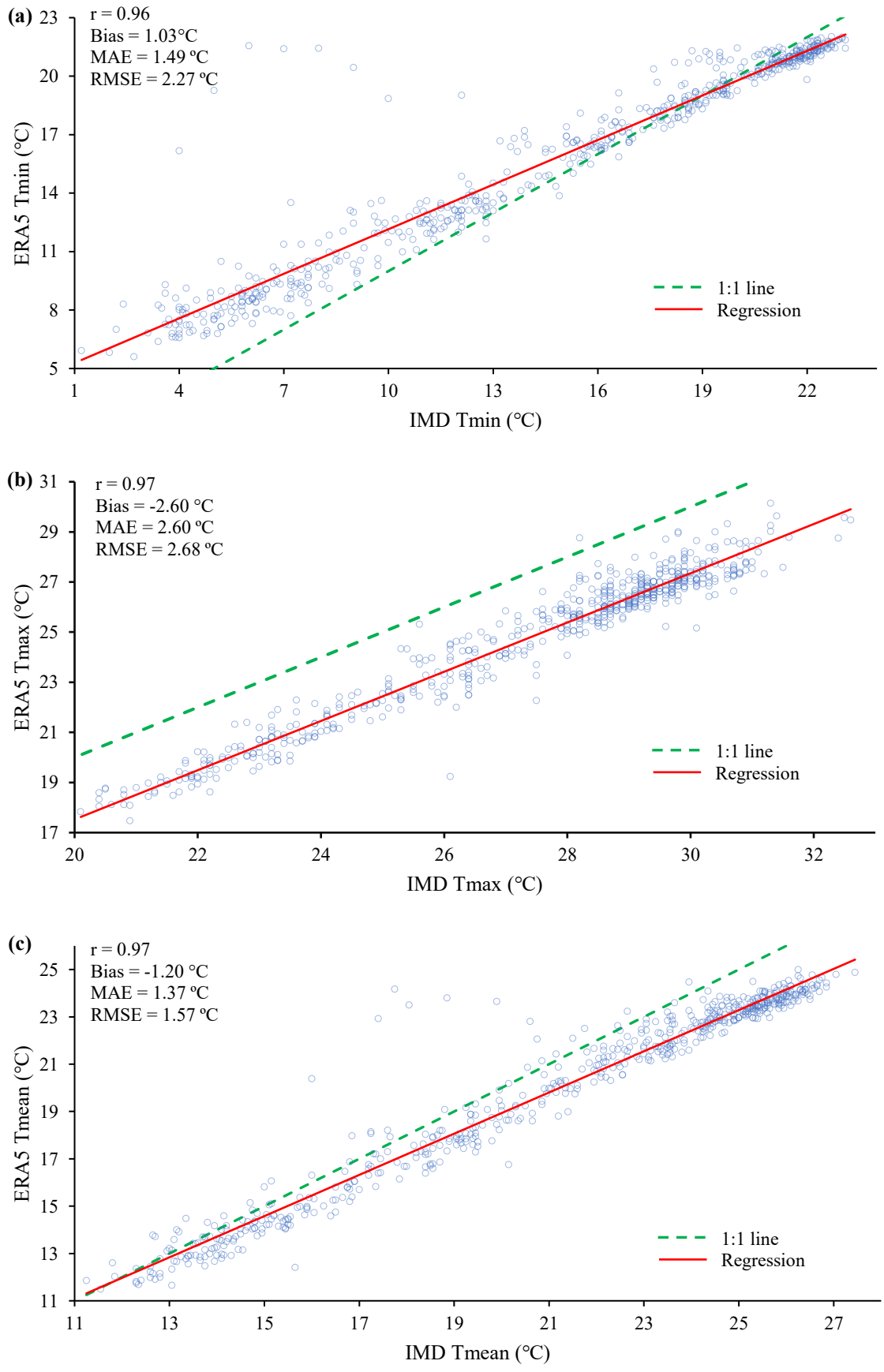



**Fig.2** Scatter plots of ERA5 monthly temperature against IMD Imphal station observations (1969–2018, n=600) for (a) Tmin, (b) Tmax, and (c) Tmean.

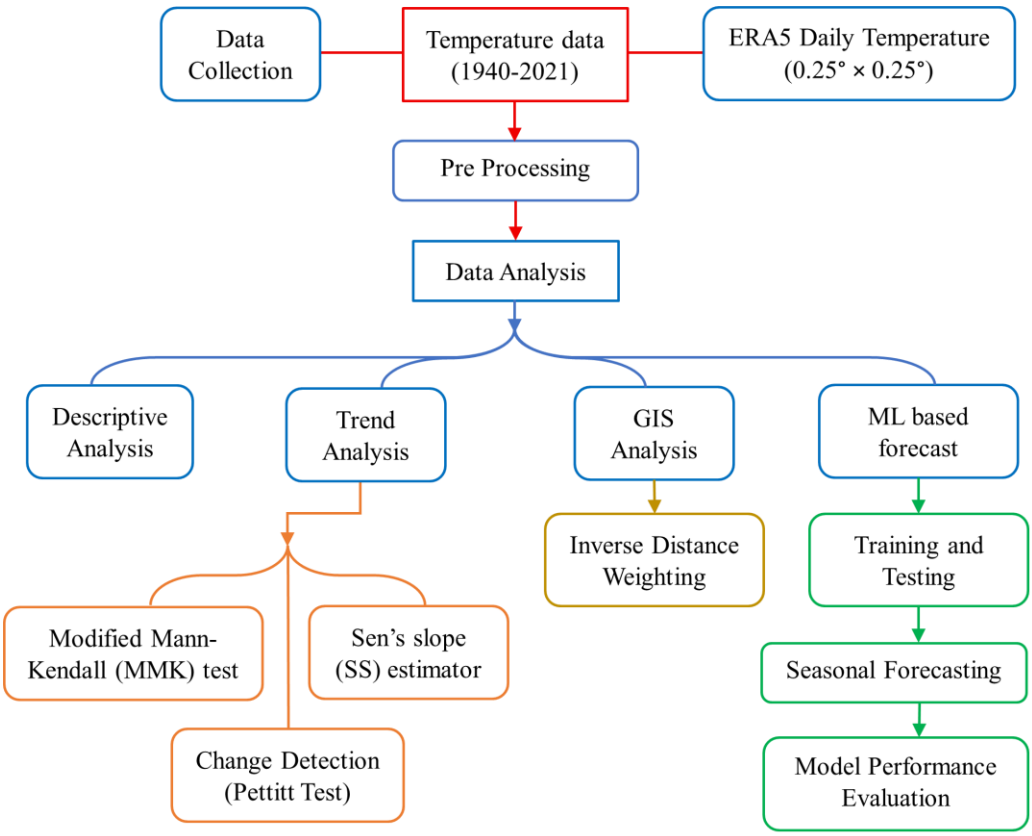



**Fig.3** Methodology flowchart

Results show strong positive lag-1 autocorrelation and persistence (r1: $T_{min}$ = 0.688, $T_{max}$ = 0.637, $T_{mean}$ = 0.665), with 11–14 of the first 19 lags ≥0.30 across variables; moreover, all lags from 1 to 19 were positive. DW tests indicate significant first-order positive autocorrelation for all three variables ($T_{min}$: DW = 1.195, $p < 0.001$; $T_{max}$: DW = 1.294, $p < 0.001$; $T_{mean}$: DW = 1.478, $p < 0.001$). Based on the decision rule ($\alpha = 0.05$), the MMK with adequate sample size variance correction was employed when either the DW test indicated significant autocorrelation or the ACF showed persistent positive correlation at early lags. Autocorrelation diagnostics were performed on the same aggregated series used for trend analysis to maintain consistency.

**Data Analysis**

The study was conducted at monthly and seasonal scales to examine variability, trends, abrupt shifts, and spatiotemporal distributions. Non-parametric trend analysis was assessed using the Modified Mann-Kendall (MMK) test and Sen's slope estimator, with Pettitt's test applied to detect significant change points over the 1940–2021 record. Seasonal temperatures — classified following IMD convention into winter, summer, monsoon, and post-monsoon were forecast for 2022–2030 using two machine learning models: Support Vector Regression (SVR) and Artificial Neural Network–Multi-Layer Perceptron (ANN-MLP). Spatial temperature patterns across Manipur were determined using Inverse Distance Weighted (IDW) interpolation. The following subsections describe the techniques in detail.

**Descriptive analysis**

The daily temperature data were analysed to observe the statistics such as mean, standard deviation, and coefficient of variance. Standard deviation indicates the extent to which the data deviates from the mean in absolute value. The coefficient of variation (CV) examines the variation in every data point from the mean, which helps assess variability. A higher CV value means a significant variability. Temperature variability is classified (Getahun et al. 2021) using the coefficient of variation (CV) into three categories: low variability (CV < 20%), moderate variability (20% < CV < 30%), and high variability (CV > 30%) CV depicts the relative variability of temperature data.

$$CV = \frac{\sigma}{\mu} \times 100 \qquad (1)$$

where, $\sigma$ = standard deviation and $\mu$ = mean

**Trend Analysis**

*Modified Mann-Kendall's test (MMK)*

Mann–Kendall (MK) test observes the size and the direction of (monotonic) trend (consistently rising or falling pattern) (Mann 1945; Kendall 1975). The Modified Mann–Kendall (MMK) test is a refinement of the classical MK test, introduced to account for autocorrelation often present in hydro-climatic datasets (Hamed & Rao, 1998). While the MK test assumes independence among observations, autocorrelation inflates the variance of its test statistic, potentially leading to false detections of trends. The MMK test corrects this issue by adjusting the variance through a practical sample size approach.

The classical MK test statistics are calculated as:

$$S = \sum_{k=1}^{n-1} \sum_{l=k+1}^{n} sig(x_l - x_k) \qquad (2)$$

Where $n$ denotes the total length of temperature data, while $x_l$ and $x_k$ are used to represent the values of the data at subsequent years.

$$sig(x_l - x_k) = \begin{bmatrix} -1, & if\ (x_l - x_k) < 0 \\ 0, & if\ (x_l - x_k) = 0 \\ +1, & if\ (x_l - x_k) > 0 \end{bmatrix} \qquad (3)$$

The S statistic is standardized to assess the statistical significance of the trend. This procedure relies on the property that for a time series of sufficient length ($n \geq 8$), the statistic approximates a normal distribution. Under the null hypothesis of no trend, the mean of the distribution, $E(S)$, is 0, and the variance, $Var(S)$, is calculated as follows:

$$Var(S) = \frac{n(n-1)(2n+5) - \sum_{p=1}^{m} t_p(t_p-1)(2t_p+5)}{18} \qquad (4)$$

where $t_p$ is the size of the $p^{th}$ group of tied observations and $m$ is the number of tied groups.

The standardized MK statistic is then given by

$$Z_s = \begin{bmatrix} \frac{S-1}{\sqrt{var(S)}}, & if\ S > 0 \\ 0, & if\ S = 0 \\ \frac{S+1}{\sqrt{var(S)}}, & if\ S < 0 \end{bmatrix} \quad (5)$$

A positive value for the $Z_s$ signifies an increasing trend, while a negative value indicates a decreasing trend. This analysis is conducted at a significance level (α) 0.05, corresponding to a 5% significance threshold. If the absolute value of $Z_s$ exceeds the critical value from the standard normal distribution, $Z_{1-\alpha/2}$ (which is 1.96 for α = 0.05), the null hypothesis of no trend is rejected.

Time series in climatology and hydrology often exhibit positive autocorrelation, especially at lower lags. This serial dependence inflates $Var(S)$ Furthermore, this leads to an overestimation of trend significance. To address this, the MMK test modifies the variance using a correction factor based on the *adequate sample size* $n_S^*$

$$\mathrm{V}^*(\mathrm{S}) = Var(S) \cdot \frac{n}{n_S^*} = \frac{n(n-1)(2n+5)}{18} \cdot \frac{n}{n_S^*} \quad (6)$$

The ratio $\frac{n}{n_S^*}$ is obtained as

$$\frac{n}{n_S^*} = 1 + \frac{2}{n(n-1)(n-2)} \sum_{j=1}^{n-1} (n-j)(n-j-1)(n-j-2) p_s(j) \quad (7)$$

where $p_s(j)$ represents the autocorrelation function of the ranks of the observations, and $n$ signifies the length of the data series. The statistical significance of any trend is determined by comparing the standardized test statistic, $Z_s$. The underlying correlation structure that defines the autocorrelation of the ranks of the observations is referred to as the parent correlation function, $p(j)$

$$p(j) = 2\ \sin\left(\frac{\pi}{6} p_s(j)\right) \quad (8)$$

*Sen's Slope Estimator*

Sen's Slope Estimator (SSE) is a robust, non-parametric method that measures the magnitude of the trend without assuming normality in the time series data. It works by calculating the median of the slopes between all possible data point pairs, ensuring reliable results even when the data contains outliers or is not normally distributed (Sen 1968).

$$Q_i = \frac{t_l - t_k}{l-k} \quad (9)$$

for all N possible pairs of data points $(t_l, t_k)$ in the series, where the time index $l > k$

The set of N slope values is then ranked in ascending order. The Sen's Slope Estimator, denoted as $Q_{med}$, is the median of this distribution.

$$Q_{med} = \begin{bmatrix} Q_{\frac{N+1}{2}}, & if\ N\ is\ odd \\ \frac{Q_{\frac{N}{2}} + Q_{\frac{N+2}{2}}}{2}, & if\ N\ is\ even \end{bmatrix} \quad (10)$$

A positive value of $Q_{med}$ signifies an increasing (upward) trend, whereas a negative value indicates a decreasing (downward) trend over the observation period. The magnitude of $Q_{med}$ represents the median rate of change.

*Pettitt test*

Pettitt test, a non-parametric statistical method developed by Pettitt (1979), assesses the occurrence of rapid changes in temperature data and helps identify abrupt changes or sudden shifts that occur in the centre of the time series data. This test is widely used for change-point detection due to its suitability for non-normally distributed data, a common characteristic of hydro-climatic variables like rainfall and temperature. The initial step begins by computing the $U_k$ statistic for each time point $k$, which is based on the Mann–Whitney ranks of the observations.

$$U_k = 2\sum_{i=1}^{k} r_i - k(n+1) \quad (11)$$

where, $r_i$ is the rank of the $i^{th}$ observation in the series, $n$ is the total number of observations, and $k$ represents the index of the potential change point.

A change point is determined to occur at the time $k$ where the absolute value of the statistic, $| U_k |$, reaches its maximum. This maximum value is defined as the test statistic $K_n$

$$K_n = max \mid U_k \mid;\ 1 \leq k \leq n \quad (12)$$

A change-point will be determined when $U_k$ attains the maximum value of $K$ in the series.

The statistical significance of this detected change point is then assessed by comparing the calculated. $K_n$ value to a critical value, $K_\alpha$ derived from the desired significance level, $\alpha$. If $K_n$ is greater than $K_\alpha$, the null hypothesis of data homogeneity is rejected.

$$K_\alpha = \sqrt{\frac{\ln(\alpha)(n^3+n^2)}{6}} \quad (13)$$

where $n$ is the number of observations, and $\alpha$ is the significance level.

**GIS Analysis**

The Inverse Distance Weighting (IDW) technique shows the spatial distribution of temperature over different periods. The spatial changes in temperature can be understood after the datasets were divided into two parts based on Pettitt's test results. IDW method assumes that data points closer to each other are more similar than those farther apart (U. Kumar et al. 2023).

**Machine Learning Models**

Traditional forecasting techniques, such as the autoregressive integrated moving average (ARIMA) and the seasonal autoregressive integrated moving average (SARIMA), are often used to predict hydrological and climatic data (Parasyris et al. 2022). These models, however, have limitations when applied to non-linear hydro-climatic datasets, including issues with serial correlation, non-linearity, and predictive bias (Canchala et al. 2020). Advanced artificial intelligence (AI) models offer a promising solution to address these challenges (Saha et al. 2020). This study employs two machine learning models: the SVR and ANN-MLP models, applied to the ERA5 dataset, to predict temperatures from 1940 to 2021. After the models achieved sufficient accuracy, they were subsequently used to forecast the next nine years, from 2022 to 2030.

*Support Vector Regression (SVR)*

A Support Vector Machine (SVM) is a robust supervised learning algorithm for classification and regression analysis (Mohammed et al. 2025; Cortes and Vapnik, 1995). For regression analysis, the algorithm is known explicitly as Support Vector Regression (SVR). SVR's fundamental principle is finding an optimal hyperplane in a high-dimensional space that best fits the data points within a specified error margin (Che Rose et al. 2025). The prediction function $f(x)$ to determine the optimal association between input data and output data is given as

$$f(x) = w^T x + b \qquad (14)$$

where $x$ is the input data vector, $w$ is the weight vector, $T$ denotes the transpose, and $b$ is the bias component. The algorithm aims to find the optimal values of $w$ and $b$ to minimize the error between the model's predictions and the actual data.

To capture complex, non-linear patterns, SVR employs a kernel function to transform the input data into a higher-dimensional feature space, where a linear separation by the hyperplane becomes possible. The data points that ultimately define the position and margin of the hyperplane are referred to as support vectors (Samantaray et al. 2020).

*Artificial Neural Network-Multilayer Perceptron (ANN-MLP)*

ANN is a machine learning algorithm modelled after the human brain's information processing system, composed of a network of interconnected nodes called neurons (Rahaman et al. 2024). A widely used ANN architecture for supervised classification and regression is the Multi-Layer Perceptron (MLP) (Mohammed et al. 2025).

The MLP consists of an input layer, one or more hidden layers, and an output layer, where each neuron receives weighted inputs from the previous layer, adds a bias term, and applies a non-linear activation function (Ahmed et al. 2020). This introduction of non-linearity is crucial, enabling the network to model complex and dynamic relationships within the data. The network learns by iteratively adjusting its connection weights using the backpropagation algorithm, which minimizes the error between the predicted and actual output values (Salaeh et al. 2022). The predicted output $y_k$ of an MLP can be expressed mathematically as:

$$y_k = f_2\left[\sum_{i=1}^{m} w_{ki} f_1\left(\sum_{j=1}^{n} w_{ij} x_j + b_i\right) + b_k\right] \qquad (15)$$

where $x_j$ represents the input variables, $w_{ij}$ and $w_{ki}$ are the connection weights between the input-hidden and hidden-output layers, respectively, $b_i$ and $b_k$ are the bias terms for the hidden and output layers, $f_1$ and $f_2$ are the activation functions for the hidden and output layers. Common choices include Sigmoid, hyperbolic tangent, or Rectified Linear Unit (ReLU), $n$ and $m$ are the number of neurons in the input and hidden layers, respectively.

**Modelling Process**

This study forecasts temperature scenarios from 2022 to 2030 using ERA5 gridded data from 1940 to 2021. Time-series forecasting employs models that analyse past data to predict future values. Seasonal climatic data were used as input to forecast temperatures for the corresponding seasons in subsequent years. The supervised machine learning model was applied to forecast seasonal temperature using historical data. Lagged features were incorporated as predictor variables to capture the temporal relationships in time series data.

In this study, two lagged variables were created: the temperature from the corresponding season in the previous year, indicating a one-year lag, and the two-year moving average of temperature, representing a two-year lagged period. Combined with the observation year and the categorical seasonal variable, these lagged features functioned as predictor variables for forecasting future temperature values. The same lag structure and input variables were consistently maintained in all models to ensure comparability and avoid differing predictor inputs. The dataset was split chronologically into training and testing sets, with 80% used for training the models and the remaining 20% allocated for testing predictive accuracy.

*Model evaluation*

The accuracy and performance of the ANN-MLP and SVR models have been assessed using four statistical evaluation metrics: the Coefficient of Determination ($R^2$), Root Mean Squared Error (RMSE), Mean Absolute Error (MAE), and Mean Squared Error (MSE) as described in Table 1. For the error-based metrics, lower values indicate higher model accuracy. The MAE quantifies the average magnitude of the errors between predicted and observed data regardless of their direction. The MSE computes the average of the squared differences, thereby placing a greater penalty on larger prediction inaccuracies. The RMSE is calculated as the square root of the MSE, which measures the average distance between the data points and the fitted regression line.

On the other hand, the $R^2$ assesses the goodness-of-fit by representing the proportion of the total variance in the dependent variable that the independent variables can explain through the regression model. Hence, a higher value signifies a better model fit to the data, whereas a lower value suggests a poorer fit. These metrics collectively provide a robust framework for quantitatively comparing the predictive power of the models.

**Table 1** Model evaluation metrics and equation

| Evaluation Metrics | Equation | Value ranges | Best Value |
|---|---|---|---|
| Coefficient of determination ($R^2$) | $R^2 = 1 - \frac{\sum_{i=1}^{N}(O_i - P_i)}{\sum_{i=1}^{N}(O_i - \bar{O})}$ | [0,1] | 1 |
| Root mean squared error (RMSE) | $RMSE = \sqrt{\frac{1}{N}\sum_{i=1}^{N}(O_i - P_i)^2}$ | [0, +∞] | 0 |
| Mean absolute error (MAE) | $MAE = \frac{1}{N}\sum_{i=1}^{N}\lvert O_i - P_i\rvert$ | [0, +∞] | 0 |
| Mean squared error (MSE) | $MSE = \frac{1}{N}\sum_{i=1}^{N}(O_i - P_i)^2$ | [0, +∞] | 0 |

Note: where $N$ is the total number of observations, $O_i$ is the observation value, and $P_i$ is the forecasted value and $\bar{O}$ is the average value of observed values

## RESULTS

### Descriptive Statistics

The temperature statistics of Manipur, India, from 1940 to 2021 are given in Table 2. The average annual temperature ($T_{mean}$) in Manipur for the last 82 years is 19.40 °C. The average $T_{min}$ is 15.28 °C, closer to $T_{mean,}$ indicating relatively cooler nights (Jhajharia and Singh 2011). On average, $T_{max}$ is 24.44 °C, which shows a

significant gap with $T_{min,}$ suggesting a substantial diurnal temperature range, a common phenomenon for mountainous states like Manipur (Vinnarasi et al. 2017).

**Table 2** Descriptive statistics of the temperature of Manipur (1940-2021)

| Variables | Mean (°C) | Standard deviation | CV (%) | Max (°C, Year) | Min (°C, Year) |
|---|---|---|---|---|---|
| Minimum ($T_{min}$) | 15.28 | 0.492 | 3.22 | 27.40 (2019) | -1.18 (1983) |
| Maximum ($T_{max}$) | 24.44 | 0.652 | 2.67 | 39.24 (1957) | 8.88 (1953) |
| Annual ($T_{mean}$) | 19.40 | 0.512 | 2.64 | 30.89 (1979) | 4.68 (1953) |

The standard deviation of all variables, $T_{min}$, $T_{max}$, and $T_{mean,}$ shows a moderate year-to-year temperature fluctuation, with values of 0.492, 0.652, and 0.512, respectively, indicating a low fluctuation of less than 1 °C. The analysis of the recorded temperature data reveals significant trends in temperature variations over time. Extreme temperature values underscore the state's climatic range. Tmin oscillates from a minimum of -1.18°C in 1983 to a peak of 27.40°C in 2019, whereas Tmax ranges from 8.88°C in 1953 to a maximum of 39.24°C in 1957. The annual Tmean followed a similar trend, with the lowest value of 4.68 °C in 1953 and the highest of 30.89 °C in 1979. Although these extremes may appear large, they are not atypical for a mountainous region with strong seasonal contrasts and elevation-driven variability. The annual maximum recorded temperatures show a $T_{min}$ of 27.40°C in 2019, a $T_{max}$ of 39.24°C in 1957, and a $T_{mean}$ of 30.89°C in 1979. While the annual lowest temperatures were documented as $T_{min}$ of -1.18°C in 1983, $T_{max}$ of 8.88°C in 1953, and $T_{mean}$ of 4.68°C in 1953. The tables provide a comprehensive overview of temperature behaviour in Manipur over the past 82 years (1940-2021).

*Temperature variability and distribution*

Table 2 presents the coefficient of variation (CV) for the three temperature parameters, providing an insightful analysis of their relative variability. Based on the classification adopted (low < 20%, moderate 20–30%, high > 30%), all three variables fall within the low-variability category (CV < 20%). This suggests that temperature changes in the region are gradual and systematic rather than erratic. All CV values are below 5%, which indicates a high degree of consistency and low relative variability in temperature trends throughout the study period. Among the parameters, the minimum temperature ($T_{min}$) exhibits the highest CV at 3.22%, suggesting a marginally greater variability in comparison to the maximum temperature ($T_{max}$) and mean temperature ($T_{mean}$). This could be attributed to greater sensitivity to nighttime climate dynamics or localized microclimatic influences.

In contrast, $T_{max}$ and $T_{mean}$ exhibit lower variability, with CV values of 2.67% and 2.64%, respectively, reflecting stable and consistent temperature patterns. The low standard deviation and CV across all analyzed variables further indicate that the temperature trends in Manipur have experienced a gradual warming trajectory. This finding reinforces the evidence of sustained, long-term climatic change in the region. The box plots (Fig. 4) illustrate Manipur's strong seasonal temperature cycle, with the lowest temperatures in winter, rising through summer, peaking during the monsoon, and then decreasing. Box plot analysis reveals notable inter-seasonal differences: summer and monsoon seasons exhibit wider interquartile ranges, indicating higher variability, while winter shows a relatively compact distribution, attesting to more stable temperature conditions. Furthermore, the presence of outliers in summer and monsoon points towards the occurrence of occasional extreme events, reinforcing the role of seasonal atmospheric dynamics in shaping temperature variability.

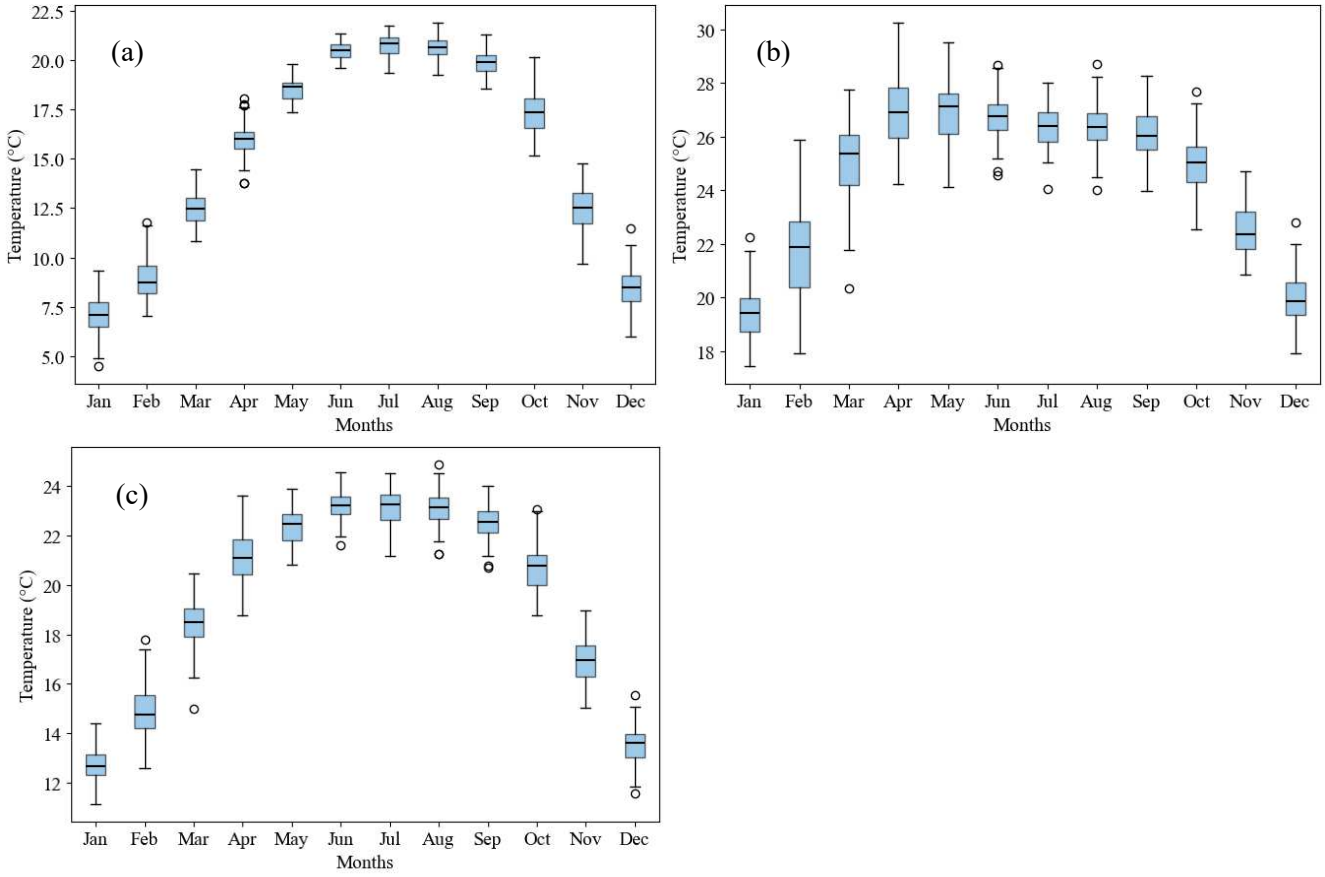



**Fig.4** Monthly temperature distribution of (a) Tmin, (b) Tmax, and (c) Tmean for Manipur (1940–2021)

## Trend Analysis

Table 3 summarizes the trend analysis results for temperature in Manipur over the 82 years from 1940 to 2021, using the non-parametric Modified Mann-Kendall (MMK) test and Sen's slope estimator. The analysis was performed at a 5% level of significance to assess long-term warming trends across three temperature variables: minimum ($T_{min}$), maximum ($T_{max}$), and mean annual temperature ($T_{mean}$).

**Table 3** Result of trend analysis for temperature (at 5% significance level) of Manipur (1940-2021)

| Categories | MMK test (Z-statistics) | Sen's slope (Q-statistics) | p-value | Trend |
|---|---|---|---|---|
| Minimum ($T_{min}$) | 3.130 | 0.016 | 0.00 | Increasing |
| Maximum ($T_{max}$) | 3.305 | 0.020 | 0.00 | Increasing |
| Annual ($T_{mean}$) | 3.609 | 0.017 | 0.00 | Increasing |

The MMK Z-statistics for all three variables are highly significant, with values of 3.130 for $T_{min}$, 3.305 for $T_{max}$, and 3.609 for $T_{mean,}$ and corresponding p-values ≤0.00, indicating robust increasing trends. Sen's slope estimator shows annual increases of 0.016°C for $T_{min}$, 0.020°C for $T_{max}$, and 0.017°C for $T_{mean}$, reflecting a steady warming trend across the decades. Over the 82-year study period, these translate into cumulative increases of approximately.

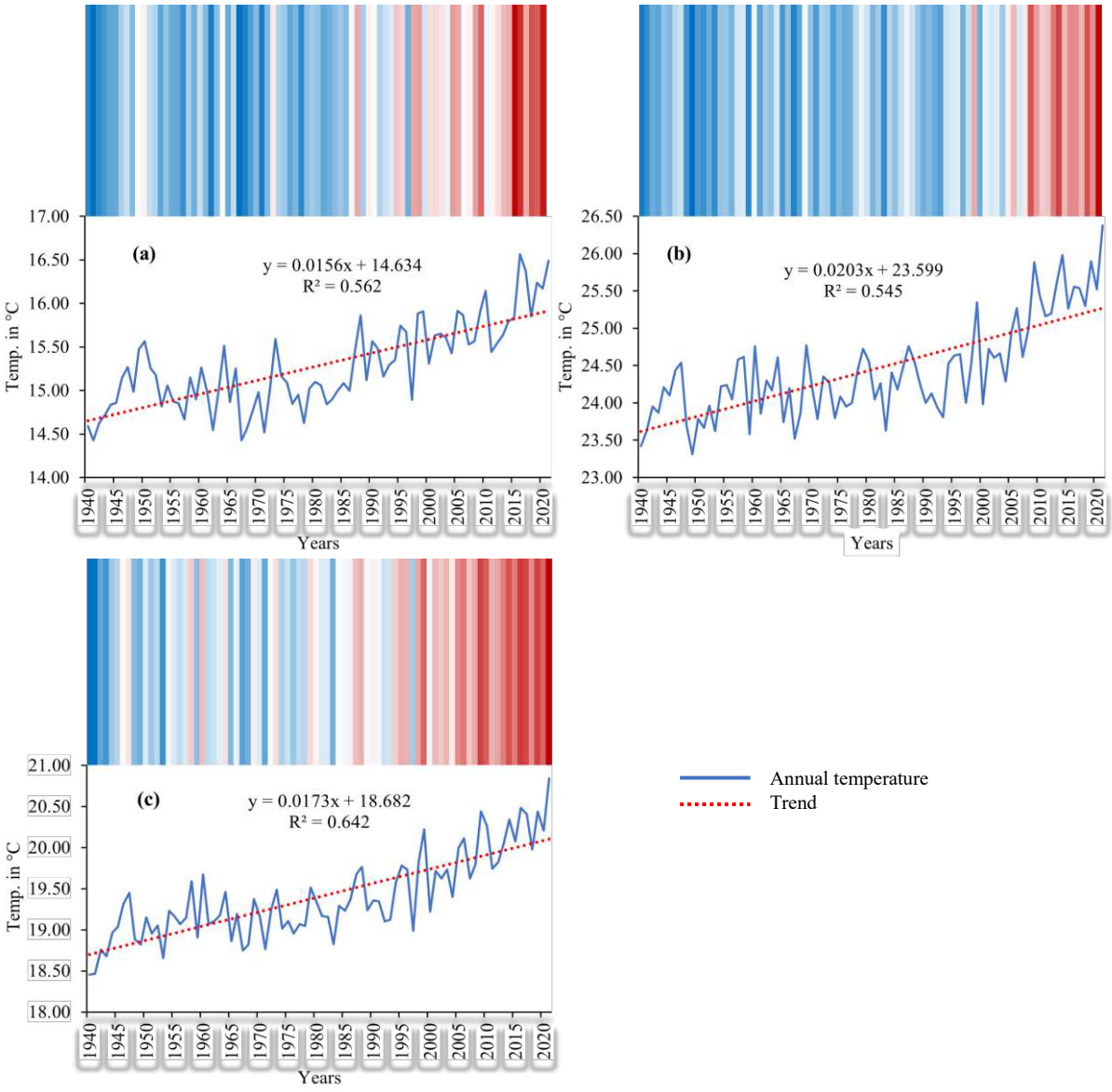



**Fig.5** Warming Stripes and temporal variation of temperature (a) Tmin, (b) Tmax, and (c) Tmean for Manipur (1940–2021) (Hawkins, 2025)

1.31 °C for Tmin, 1.64 °C for Tmax, and 1.39 °C for Tmean, underscoring a substantial long-term warming signal. The relatively greater increase in Tmax suggests that daytime temperatures are rising faster than nighttime temperatures, indicating an intensification of heat conditions.

Further, the linear regression analysis supports these findings, with coefficient of determination ($R^2$) values of 0.562, 0.545, and 0.642 for Tmin, Tmax, and Tmean, respectively. These values demonstrate that long-term trends explain a significant proportion of temperature variability. Tmean shows the most consistent and pronounced warming, indicated by a high $R^2$ value. The warming stripes (Fig. 5) visualize the observed long-term temperature

changes in the study area and closely mirror the linear trends. The warming stripes are coloured stripes—blue indicates cooler years and red indicates warmer years than the average value (Hawkins 2025). It shows a progressive transition from cooler to warmer years, particularly after the 1980s.

*Change point analysis*

The Pettitt's test was applied to detect a change point in Manipur's monthly temperature data set. The test results identified change points for the $T_{min}$, $T_{max,}$ and $T_{mean}$ trends as 1985, 1992, and 1984, respectively. This result reveals a significant warming post-1980s, with accelerated rises in recent decades. A comparison of pre- and post-change periods reveals substantial temperature increases. $T_{min}$ rose from 14.96 °C in 1940–1985 to 15.69 °C in 1986–2021, marking an increase of 0.73 °C, while $T_{max}$ increased from 24.11 °C in 1940–1992 to 25.04 °C during 1993–2021, reflecting a rise of 0.93 °C. Similarly, $T_{mean}$ climbed from 19.07 °C in 1940–1984 to 19.80 °C in 1985–2021, indicating a warming of 0.73 °C (Fig. 6). Tmax shows the largest change, reinforcing the finding of stronger daytime warming.

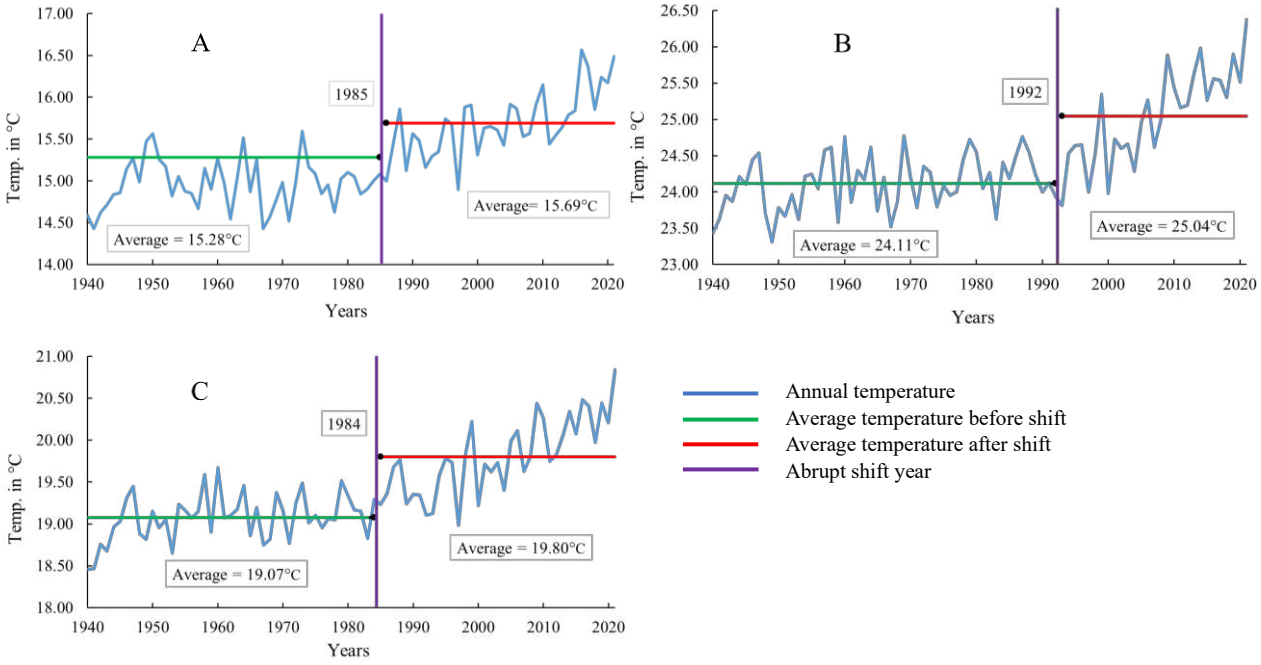



**Fig. 6** Graphical representation of Pettitt's test used for detecting change points in temperature trend of (A) Tmin, (B) Tmax, and (C) Tmean for Manipur

These change points align closely with the globally observed acceleration of warming since the 1980s, widely attributed to increased greenhouse gas concentrations and regional climate feedback mechanisms. Similar post-1980s warming trends have been recorded in Northeast India (Gautam et al. 2025), indicating this observed shift is part of a broader regional and global climatic transition. Figure 6 further illustrates these changes, revealing a distinct inflection point in the time series and a clear upward shift in mean temperature after the identified breakpoints. The step-like elevation in the post-change mean line further confirms a regime shift rather than a gradual linear progression.

**Assessment of spatial change**

The long-term temperature dataset for Manipur was divided into two distinct periods based on the change points identified through Pettitt's test: 1940–1985 and 1986–2021 for $T_{min}$, 1940–1991 and 1992–2021 for $T_{max,}$ and 1940–1984 and 1985–2021 for $T_{mean}$. Following this division, Inverse Distance Weighted (IDW) interpolation was incorporated to generate spatial distribution maps for each segment, illustrating the monthly variations in minimum ($T_{min}$), maximum ($T_{max}$), and mean ($T_{mean}$) temperatures across the state. The maps used a color-coded scheme to display temperature variation, with dark red indicating the highest temperature value and cool green highlighting the lowest. This approach makes it easy to see how temperature patterns are distributed across different parts of Manipur during the studied periods.

*Minimum Temperature ($T_{min}$)*

The spatial distribution of minimum temperature ($T_{min}$) across Manipur from January to December (Figure 6) shows a statewide warming trend when comparing the 1940–1985 and 1986–2021 periods. The most pronounced shifts are concentrated in the transitional months at either end of the winter season. February exhibits the largest warming, with a statewide mean increase of +0.99°C (from 8.45°C to 9.44°C). This month also represents the most dramatic spatial transformation across all regions. The central valley shows the sharpest increase of up to 1.05 °C. The widespread replacement of green-shaded areas (6.2–8.0°C) in the 1940–1985 maps by orange and red hues (7.1–9.5°C) in the 1986–2021 period is evident (Fig.7). October and November experience the next most substantial warming at +0.92°C and +0.85°C, respectively. During these post-monsoon months, the western region — comprising Jiribam (Imphal East) and Churachandpur districts — shows a prominent expansion of orange and red zones (15.1–20.9°C in October; 10.2–15.9°C in November) that were absent earlier. The southwestern region records an annual average $T_{min}$ warming of +0.88°C, the highest of any sub-region, confirming the western fringe as a consistent warming hotspot across the post-1986 period.

In contrast, the months of April (+0.46°C) and May (+0.44°C) manifest comparatively subdued shifts. The spatial maps for these summer months show only minor color transitions between the two periods, with the distribution of green and orange hues remaining broadly similar, suggesting that nighttime temperatures during the pre-monsoon period have been less sensitive to the post-1985 regime shift. The northeast highlands, including Ukhrul district and its eastern reaches, consistently show the smallest warming increases across all months, with an annual average difference of +0.66°C, approximately 0.22°C lower than in the most affected southwestern areas.

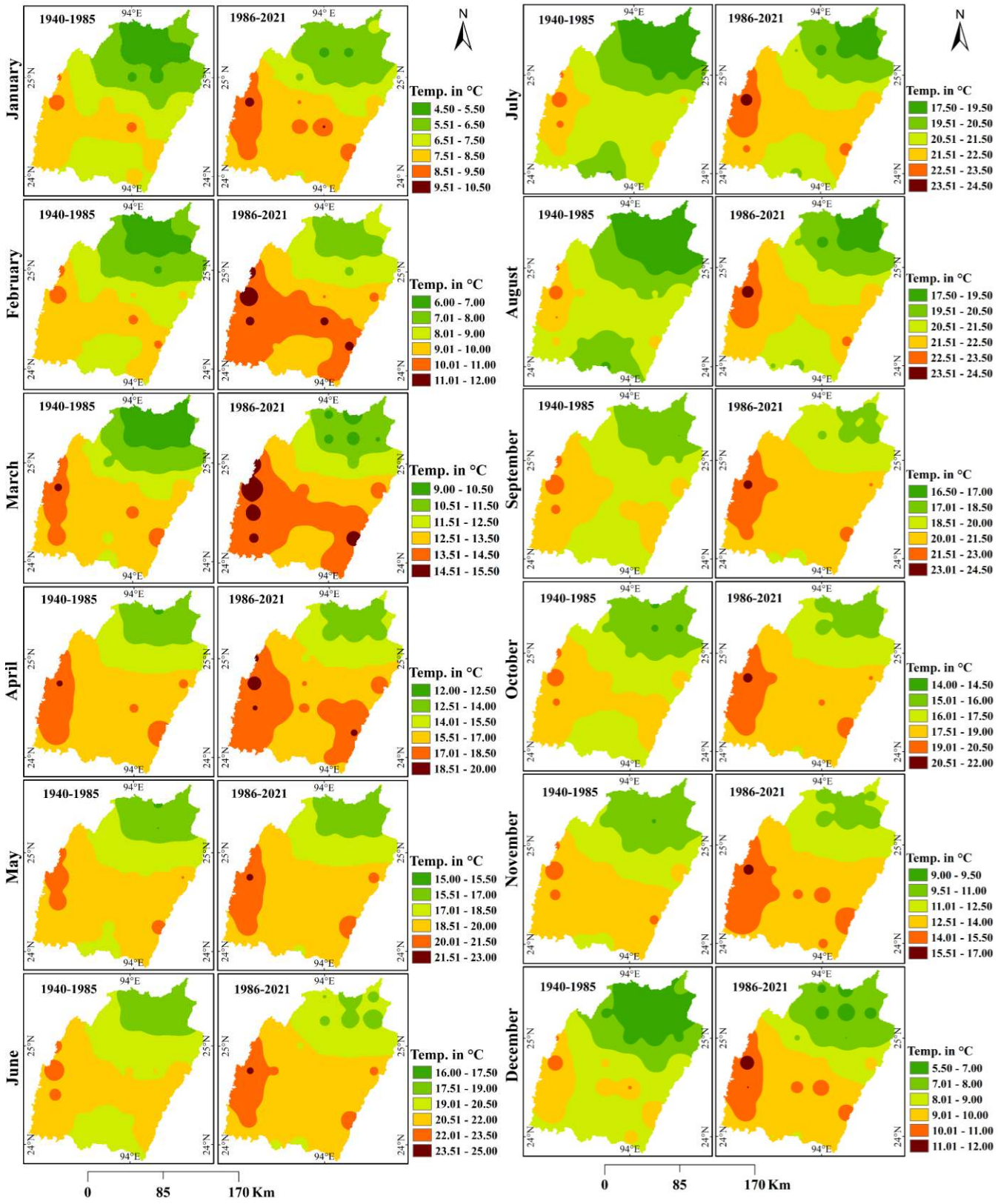



**Fig. 7** Spatial distribution of Tmin in Manipur from January to December

479

480 .

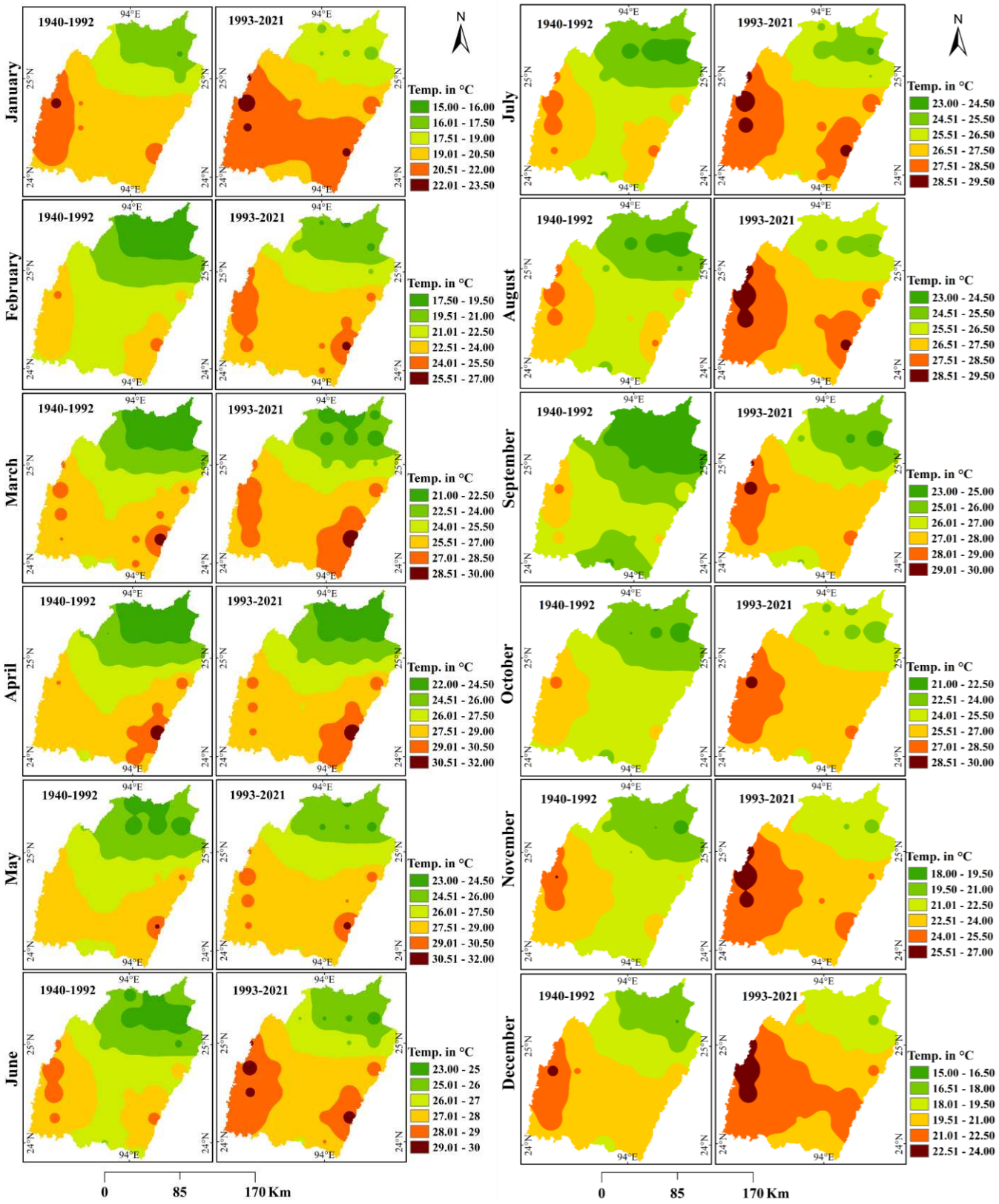



**Fig.8** Spatial distribution of Tmax in Manipur from January to December

481

482

*Maximum Temperature ($T_{max}$)*

Figure 8 illustrates the spatial changes in maximum temperature ($T_{max}$) in Manipur, comparing 1940–1992 with 1993–2021. A distinct upward trend is observable throughout the year. In the winter and pre-monsoon months from January to May, the maps for the post-1993 period consistently show an expansion of areas shaded in orange, red, and dark red, signifying higher maximum temperatures. The shift is particularly notable in April and May, when orange and red areas (27.51°C to 30.50°C) become more prominent in the central and eastern parts of the state. During the monsoon months of June, July, August, and September, the warming pattern persists, with the 1993–2021 maps displaying more widespread orange and red shading (26.51°C to 30.00°C) compared to the earlier period. A significant increase in $T_{max}$ is seen in the post-monsoon months. The map for October in the 1993-2021 period shows large patches of dark red (28.51°C to 30.00°C) that were absent in the 1940-1992 map. Similarly, November and December in the later period show a marked increase in the extent of orange and red areas, indicating substantially higher maximum temperatures across the state.

*Mean Temperature ($T_{mean}$)*

The spatiotemporal distribution of the mean temperature ($T_{mean}$) for the 1940–1984 and 1985–2021 periods is shown in Fig. 9. The analysis reveals a clear and consistent increase in mean temperatures across all twelve months. Beginning with January, the post-1985 map shows a definite shift to warmer temperatures, with orange and red areas (13.01°C to 15.00°C) replacing the cooler green shades of the earlier period. This warming trend becomes more pronounced from February to May, with the maps for the 1985-2021 period showing a significant expansion of red and dark red areas, particularly in March. The monsoon months from June to September continue to display this warming pattern. The maps for the later period are visibly warmer, dominated by orange and red hues (23.01°C to 26.50°C) and showing an apparent increase from the mean temperatures recorded in the 1940–1984 period. The temperature rise is also very evident in the post-monsoon and winter months. In October and November, the 1985-2021 map features large areas of dark red which were not present previously, while December shows a similar shift towards warmer orange and red shades. These results highlight a consistent warming pattern in Manipur's climate over the recent decades.

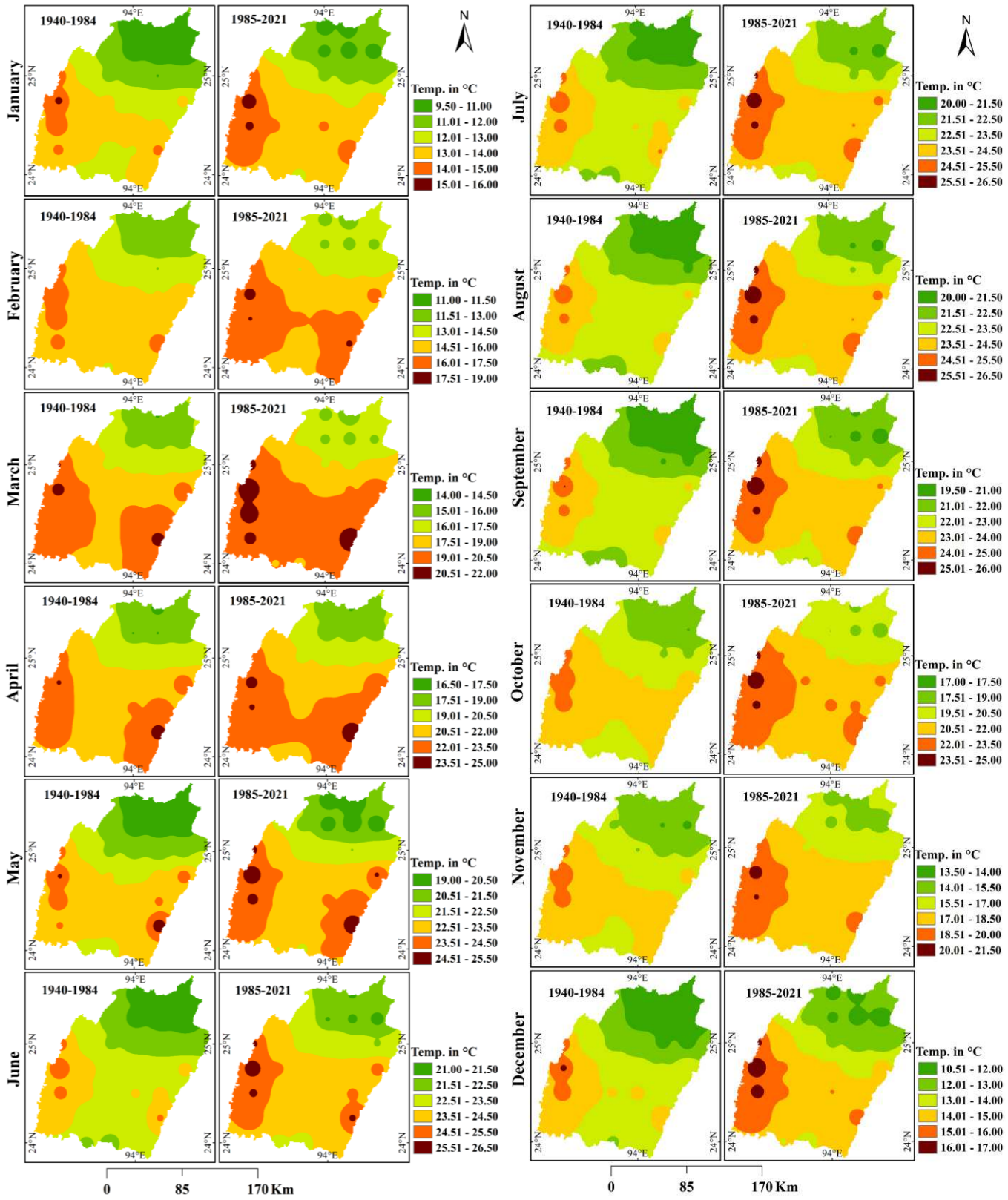



**Fig.9** Spatial distribution of Tmean in Manipur from January to December

**Seasonal forecast of temperature variables**

The temperature variables were predicted (1940-2021) and then forecasted (2022-2030) using the ANN-MLP and the SVR in this study. The comparative seasonal forecast plots for 2022-2030 are presented in the Figs. 10, 11, and 12.

*Model Performance Evaluation*

The predictive performance of two machine learning models, ANN-MLP and SVR, was assessed for forecasting $T_{min}$, $T_{max,}$ and $T_{mean}$ across four seasons. In the Table 4, the results show that the SVR model is superior for predicting $T_{min}$. Across all four seasons, SVR consistently achieved higher $R^2$ values (approaching 1.0) and significantly lower error metrics (RMSE, MAE, and MSE) when compared to ANN-MLP. A similar pattern of SVR dominance was observed for $T_{mean}$, where it outperformed ANN-MLP in three seasons: Winter, Summer, and Post Monsoon.

However, the evaluation for $T_{max}$ indicated a more complex, season-dependent result. While the SVR model achieved higher accuracy during the Winter, the ANN-MLP model proved effective for the rest, with lower error values. Therefore, while SVR is the superior model for $T_{min}$ and the most robust choice for $T_{mean}$, the optimal model for $T_{max}$ forecasting depends on the specific season.

**Table 4** Comparison of the forecasting model performance of the ANN-MLP and SVR

| Seasons | Evaluation Metrics | $T_{min}$ | | $\boldsymbol{T_{max}}$ | | $\boldsymbol{T_{mean}}$ | |
|---|---|---|---|---|---|---|---|
| | | ANN-MLP | SVR | ANN-MLP | SVR | ANN-MLP | SVR |
| Winter | Coefficient of determination ($R^2$) | 0.9997 | **1.0000** | 0.9999 | **1.0000** | 0.9992 | **0.9999** |
| | Root mean squared error (RMSE) | 0.0115 | **0.0041** | 0.0079 | **0.0045** | 0.0186 | **0.0050** |
| | Mean absolute error (MAE) | 0.0097 | **0.0035** | 0.0078 | **0.0037** | 0.0171 | **0.0039** |
| | Mean squared error (MSE) | 0.0001 | **0.0000** | 0.0001 | **0.0000** | 0.0003 | **0.0000** |
| Summer | Coefficient of determination ($R^2$) | 0.9958 | **0.9999** | 1.**0000** | 1.0000 | 0.9995 | **0.9999** |
| | Root mean squared error (RMSE) | 0.0287 | **0.0048** | **0.0009** | 0.0035 | 0.0103 | **0.0041** |
| | Mean absolute error (MAE) | 0.0222 | **0.0037** | **0.0007** | 0.0026 | 0.0092 | **0.0034** |
| | Mean squared error (MSE) | 0.0008 | **0.0000** | **0.0000** | 0.0000 | 0.0001 | **0.0000** |
| Monsoon | Coefficient of determination ($R^2$) | 0.9600 | **0.9975** | **1.0000** | 0.9995 | **0.9989** | 0.9987 |
| | Root mean squared error (RMSE) | 0.0363 | **0.0091** | **0.0013** | 0.0077 | **0.0074** | 0.0081 |
| | Mean absolute error (MAE) | 0.0308 | **0.0090** | **0.0012** | 0.0076 | **0.0063** | 0.0080 |
| | Mean squared error (MSE) | 0.0013 | **0.0001** | **0.0000** | 0.0001 | **0.0001** | 0.0001 |
| Post Monsoon | Coefficient of determination ($R^2$) | 0.9992 | **0.9999** | **1.0000** | 1.0000 | 0.9999 | **1.0000** |
| | Root mean squared error (RMSE) | 0.0181 | **0.0045** | **0.0008** | 0.0015 | 0.0047 | **0.0031** |
| | Mean absolute error (MAE) | 0.0160 | **0.0037** | **0.0007** | 0.0012 | 0.0039 | **0.0026** |
| | Mean squared error (MSE) | 0.0003 | **0.0000** | **0.0000** | 0.0000 | 0.0000 | **0.0000** |

**Seasonal forecast of $\boldsymbol{T_{min}}$**

The SVR model predicts a steadily declining trend for the winter season, with $T_{min}$ decreasing from 8.72°C in 2022 to 8.48°C in 2030. In contrast, the ANN-MLP model forecasts a near-constant $T_{min}$, showing only a minor fluctuation from 8.89°C to 8.90°C over the same period. Both models predict high variability in the summer season with peaks and troughs. The SVR model forecasts a slight increase, from 15.73°C in 2022 to 15.87°C in 2030, with a peak of 16.52°C in 2023. On the contrary, the ANN-MLP model forecasts a slight decrease in $T_{min}$ from 15.62°C in 2022 to 15.48°C in 2030, though it also shows significant variability. During the monsoon season, both models forecast a declining trend for $T_{min}$. The ANN-MLP model exhibits a gentle decrease with low

variability, whereas the SVR model forecasts a more pronounced and steady decline, from 21.24°C in 2022 to 20.84°C in 2030. For the post-monsoon season, the two models show completely divergent forecasts. The ANN-MLP model predicts a steady decline from 14.26°C to 14.09°C. The SVR model, however, forecasts a significant and steady rise in $T_{min}$, increasing by approximately 11% from 14.34°C in 2022 to 15.92°C in 2030

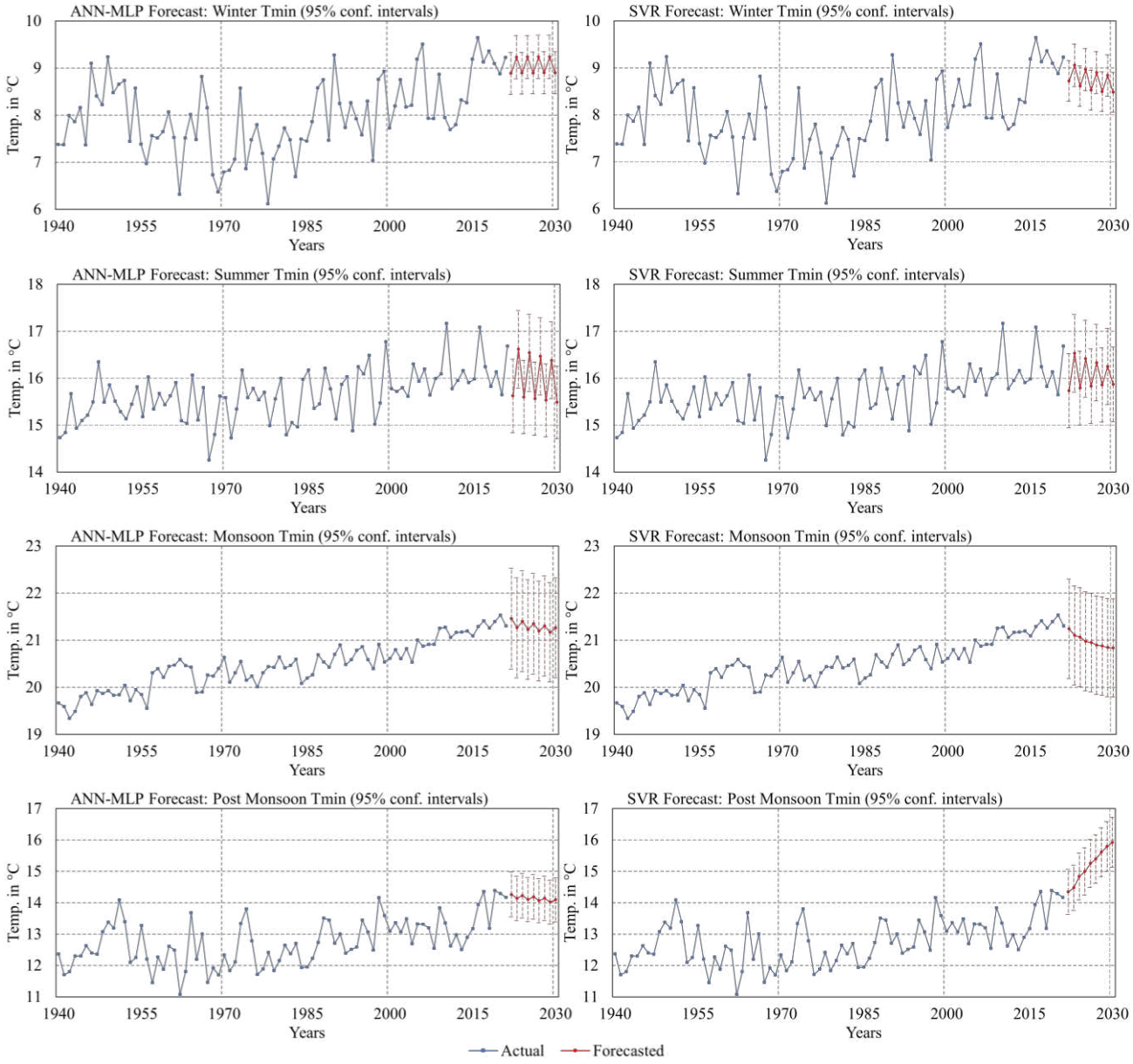



**Fig. 10** Seasonal forecast of Tmin (2022-2030)

**Seasonal forecast of $T_{max}$**

Both models forecast a slight increase in $T_{max}$ in the winter season with low variability. The ANN-MLP model predicts a rise from 21.11°C in 2022 to 21.59°C in 2030, while the SVR model shows a similar, albeit marginal, increase. Both models forecast an increasing trend for $T_{max}$ for the summer season, characterized by high

variability. The ANN-MLP forecast shows $T_{max}$ rising from 26.80°C to 26.90°C, with a significant peak of 28.86°C in 2026. The SVR model also predicts a rising trend with multiple peaks and troughs over the forecast period.

During the monsoon season, both models forecast a declining trend in $T_{max}$. The ANN-MLP forecast shows a decrease from 27.42°C in 2022 to 26.99°C in 2030. Similarly, the SVR model predicts a steady decline with relatively low variability. In the post-monsoon season, the ANN-MLP and SVR models forecast a slight increase in $T_{max}$ over the years. The ANN-MLP model predicts a rise from 24.47°C in 2022 to 24.99°C in 2030, while the SVR model shows a similar upward trend, indicating a consensus on warming for this season.

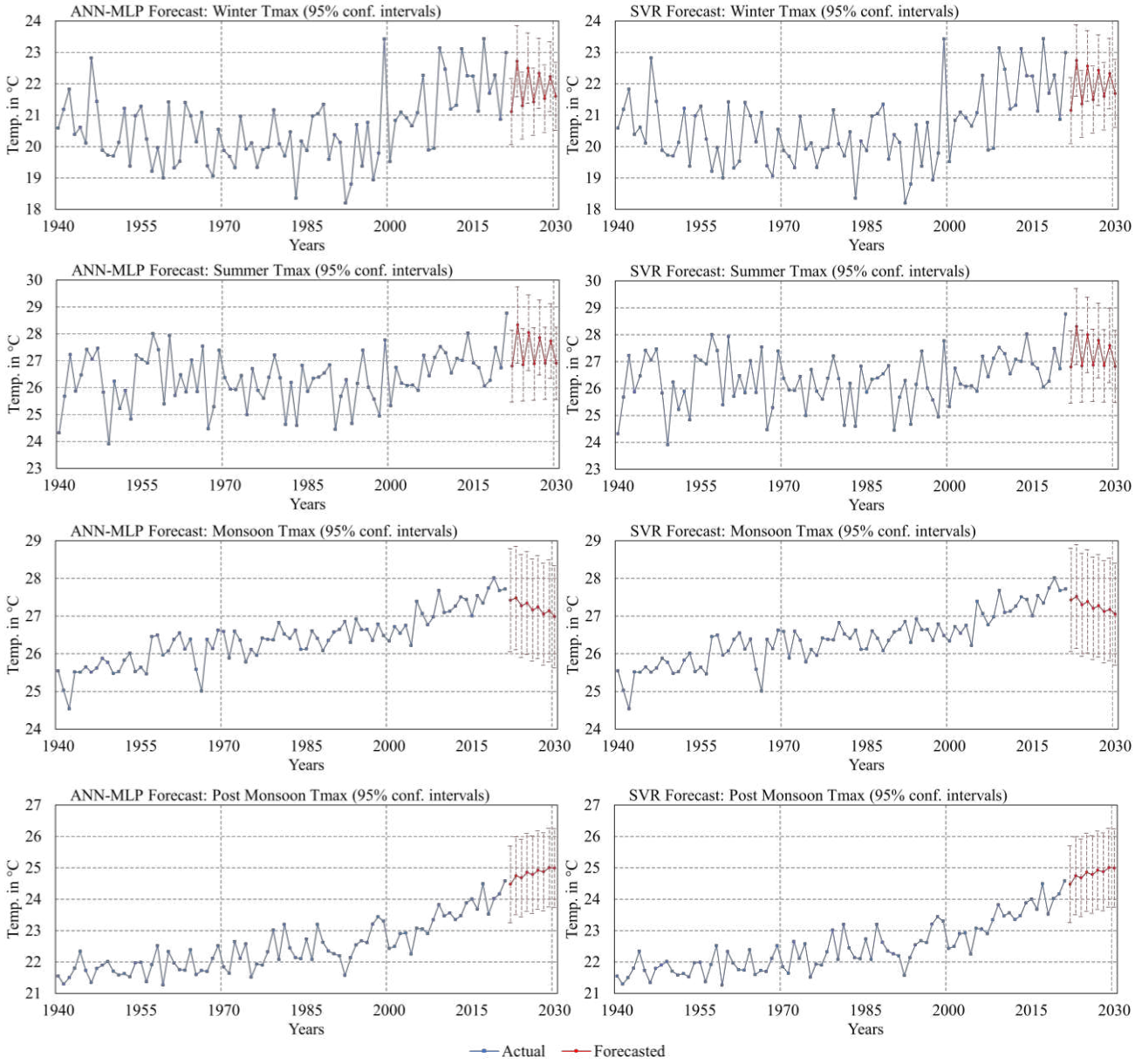



**Fig. 11** Seasonal Forecast of Tmax (2022-2030)

**Seasonal forecast of $T_{mean}$**

Both models predict a small but steady rise in $T_{mean}$ for the winter seaso$_n$ with very low variability. The ANN-MLP forecast shows an increase from 14.16°C in 2022 to 14.89°C in 2030, a trend mirrored by the SVR model's predictions. Both models forecast a steadily increasing $T_{mean}$ with high variability in the summer season. The ANN-MLP model predicts an increase from 20.82°C to 20.93°C, with a prominent peak in 2023 at 22.12°C. However, the SVR model forecasts a slight decrease from 20.79°C in 2022 to 20.76°C in 2030 with significant year-to-year fluctuations.

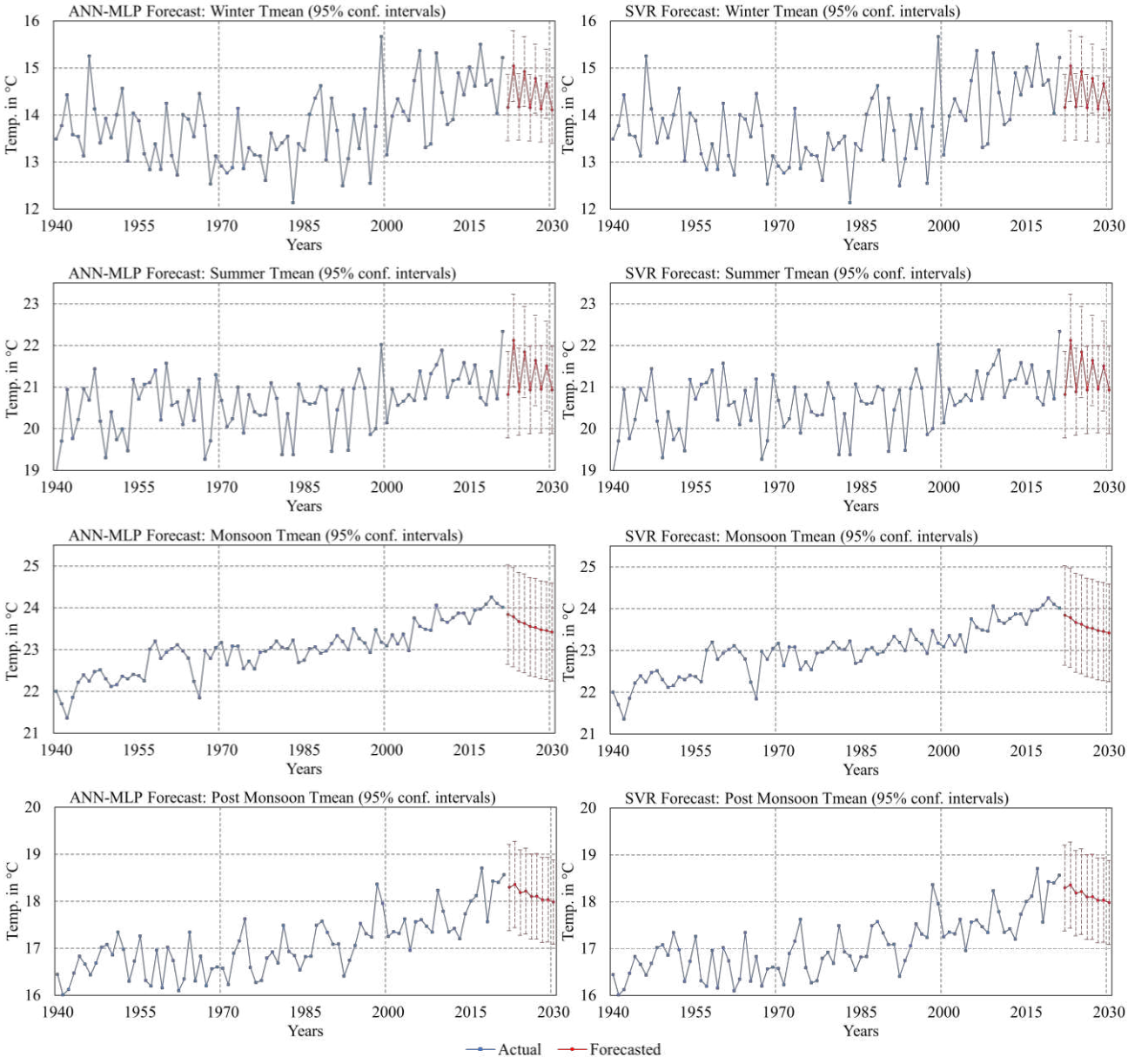



**Fig. 12** Seasonal forecast of Tmean (2022-2030)

The MLP and SVR models forecast a clearly declining $T_{mean}$ trend for the monsoon season. The ANN-MLP model shows a decrease from 23.84°C to 23.42°C, and the SVR model predicts a similar steady decline over the nine years. During the post-monsoon season, both models forecast a consistent decline in $T_{mean}$ with moderate variability. The ANN-MLP model predicts a decrease from 18.32°C in 2022 to 17.96°C in 2030. The SVR model also forecasts a clear decreasing trend, with $T_{mean}$ falling from 18.29°C to 17.98°C cover the forecast period. Overall, a decrease in $T_{mean}$ is forecasted for the monsoon and post-monsoon seasons.

**Discussion**

The trend analysis results demonstrate a clear and statistically significant warming trajectory across Manipur over the 1940–2021 period, with annual Tmax exhibiting the highest rate of increase (0.020°C/year), followed by Tmean (0.017°C/year) and Tmin (0.016°C/year). These findings are consistent with the accelerating warming signal documented across Northeast India and the broader eastern Himalayan region (Gautam et al. 2025; Banerjee et al. 2025). Notably, the relatively higher rate of Tmax warming compared to Tmin suggests a tendency toward an alteration in the traditionally observed diurnal asymmetric warming pattern, wherein nocturnal minimum temperatures historically warmed faster than daytime maxima (Vose et al. 2005). The higher rate of Tmax warming is consistent with Zhong et al. (2023), who reported faster increases in daytime temperatures in many regions due to reduced cloud cover, increased solar irradiance (global brightening), and land–atmosphere feedbacks associated with droughts and heatwaves. While the present analysis does not explicitly examine these driving mechanisms, the observed Tmax-dominant warming in Manipur may reflect similar processes operating at the regional scale. The warming rates observed in Manipur thus reflect both regional manifestation of global climate forcing and a shift in diurnal temperature dynamics, with important implications for heat stress, evapotranspiration, and climate-sensitive ecosystems.

Pettitt's test indicates that temperature changes over Manipur are non-secular, with significant change points at 1984 (Tmean), 1985 (Tmin), and 1992 (Tmax), marking a transition to an accelerated warming phase consistent with earlier findings from Northeast India (Jain et al. 2013). The clustering of these breakpoints during the mid-1980s to early 1990s aligns with the global climate regime shift of the 1980s associated with intensified greenhouse forcing and recovery from the 1982 El Chichón volcanic eruption (Reid et al. 2016; IPCC 2021). The earlier change points for Tmin (1985) and Tmean (1984), relative to Tmax (1992), reflect the established pattern of greenhouse-driven warming, wherein minimum temperatures respond more rapidly due to enhanced longwave radiation trapping, cloud-mediated insulation, and shallow nighttime boundary layer effects (Liu et al. 2024). The later Tmax breakpoint in 1992 may additionally relate to post-eruption warming following the 1991 Mount Pinatubo eruption, which temporarily suppressed daytime temperatures before a rebound. Importantly, this earlier Tmin response does not contradict the higher long-term Tmax warming rate; rather, change points capture the timing of initial responses, while trend magnitudes reflect cumulative warming, consistent with recent evidence of increasing Tmax dominance in global temperature trends (Zhong et al. 2023; Vose et al. 2005). Regional studies further identify temperature regime shifts across Northeast India (Gautam et al. 2025), though the earlier breakpoints in Manipur suggest that climate reorganisation in the state preceded the broader early twenty-first century shift, highlighting spatial and temporal heterogeneity in warming across the eastern Himalayan region (S.T.P. Kumar et al. 2023).

The spatial analysis of the temperature change reveals a heterogeneous warming pattern across Manipur, with the most pronounced Tmin increases observed in the western and southwestern districts, particularly Jiribam and Churachandpur (+0.88°C), while the northeastern highlands such as Ukhrul exhibit comparatively lower warming (+0.66°C). This gradient indicates stronger warming in lower-elevation transitional zones than in higher-elevation areas, deviating from the typical elevation-dependent warming (EDW) hypothesis (Pepin et al. 2025). Instead, it shows complex patterns of warming in mountainous regions with strong microclimatic influence (Pepin et al. 2015). We hypothesise that the enhanced warming in the western lowlands likely reflects the combined influence of topographic exposure to warm, moisture-laden air masses from the Bay of Bengal and intensified land surface heating associated with lower elevations and land-use changes. The pronounced post-monsoon warming in these regions further suggests delayed heat release from the monsoon season, a process less evident in cooler highland areas. However, the pre-monsoon Tmax pattern shows relatively stronger warming in central and eastern regions, indicating a partial seasonal influence of solar radiation amplification at higher elevations (Gautam et al. 2009). Overall, the findings suggest that warming patterns in Manipur are governed by the interaction of elevation, terrain exposure, and regional atmospheric processes rather than elevation alone, highlighting the importance of local controls in shaping climate variability across the region.

We find that both forecasting models, SVR and ANN-MLP, demonstrated strong predictive performance across all seasonal temperature variables in Manipur. The generally superior performance of SVR for Tmin and Tmean across most seasons is consistent with its well-documented structural advantage in limited-sample time-series forecasting (Ateeq-ur-Rauf et al. 2018). SVR typically requires fewer calibration samples than ANN models to achieve reliable predictive performance, which is particularly relevant in the present study based on an 82-year seasonal dataset (Tange et al. 2017). These findings are broadly consistent with previous studies applying non-parametric and ensemble-based machine learning approaches for seasonal temperature forecasting in similar regions. For instance, Roshani et al. (2022), using a Random Forest model for temperature forecasting in the Himalayan foothills of the Valmiki Tiger Reserve with IMD gridded data, reported R values ranging from 0.819 to 0.979 across different seasons and variables. Similarly, Rahaman et al. (2024), in a meteorological forecasting study in the lower Thoubal watershed of Manipur, reported $R^2$ values between 0.882 and 0.961 across most seasons and variables. Overall, the results suggest that conventional ANN architectures may underperform relative to SVR and other advanced machine learning techniques in data-limited mountain regions of India, closely aligning with the findings of the present study. This provides further support for the modelling approach adopted in this research.

The projected warming during the winter and summer seasons in Manipur will have a significant impact on the four sectors (agriculture, forests, water resources, and human health) identified in Manipur's State Action Plan on Climate Change (SAPCC 2013) as vulnerable to climate change. The correspondence between the most pronounced warming in the western and southwestern regions of the state and areas previously identified as highly climate-vulnerable in composite environmental and socioeconomic vulnerability assessments (Elangbam and Singh 2025) suggests that existing socioeconomic and environmental stresses in these districts may be further intensified under continued warming. Rising winter temperatures may disrupt the timing and productivity of rabi crops by altering optimal sowing and maturation windows, particularly in the valley agricultural systems. Increased summer temperature projections suggest that the pre-monsoon dry period will be under greater evapotranspiration stress, reducing soil moisture availability and increasing irrigation demand in rain-fed

agricultural areas already under seasonal water stress. Sustained warming may place additional thermal stress on the Loktak Lake ecosystem, a Ramsar-designated wetland of international importance, potentially affecting aquatic biodiversity, water quality, and the livelihoods of fishing communities dependent on it. Furthermore, there is a likelihood of a decline in seasonal rainfall reliability in rain-fed upland streams that support domestic and agricultural water supply across Manipur's hill and valley districts, with adverse consequences for water security and public health in rural communities. Finally, the temperature projections presented in this study provide credible, local evidence supporting the urgency of adopting targeted climate adaptation across different regions of the state.

This study has limitations related to data availability, spatial resolution, and modelling uncertainty. The ERA5 data validation was performed using a single IMD observation station due to the unavailability of accredited observational infrastructure in the state. The high correlation between the observation and ERA5 data, however, makes it appropriate for long-term trend analysis. The study acknowledges limitations imposed by the coarse 0resolution of ERA5 data, especially when interpolation is done in a topographically complex region like Manipur. Additionally, the deterministic SVR and ANN-MLP models do not quantify forecast uncertainty, highlighting the need for probabilistic approaches in future studies.

**Conclusion**

Evaluating past and future temperature changes in data-sparse mountainous regions experiencing rapid climate change is essential for formulating informed climate policies. This study assessed long-term temperature changes in Manipur by combining traditional statistical and geospatial mapping techniques with machine-learning forecasting, an analytical framework with replicability potential for analogous data-scarce areas within the broader eastern Himalayan region. Statistically significant warming was observed in annual Tmin (0.016°C/year), Tmax (0.020°C/year), and Tmean (0.017°C/year) across the 1940–2021 period, with the higher Tmax rate suggesting a tendency toward reversal of the traditionally observed diurnal asymmetric warming pattern. Distinct temperature regime shifts concentrated in the mid-1980s to early 1990s marked a transition to an accelerated post-shift warming phase that has persisted through the study period. Spatiotemporal analysis revealed uneven warming, with the western and southwestern districts, coinciding with Manipur's most climate-vulnerable districts, experiencing stronger warming than the northeastern highlands. Machine learning-based forecasting projects continued warming across summer and post-monsoon seasons for 2022–2030, with model uncertainty reflected in the inter-model divergence in winter Tmin forecasts. The climate-related risks to agriculture, water resources, forest ecosystems, biodiversity, and human health, the four most climate vulnerable sectors in Manipur, are expected to increase as warming continues. The results emphasise the need to formulate and implement evidence-based climate adaptation strategies to promote climate-resilient agriculture, water management, ecosystem conservation, and improved climate monitoring in the state's most vulnerable districts. Future studies should incorporate additional impact variables, higher-resolution spatial downscaling, and probabilistic forecasting frameworks to build upon the framework presented by this study.

## References


Ahamed MRA, Maharana P, Dimri AP (2024) Elevation dependency of precipitation and temperature over northeast India. Theoretical and Applied Climatology 155(7):6409–6426. https://doi.org/10.1007/S00704-024-05019-0

Ahmed K, Sachindra DA, Shahid S, Iqbal Z, Nawaz N, Khan N (2020) Multi-model ensemble predictions of precipitation and temperature using machine learning algorithms. Atmospheric Research 236:104806. https://doi.org/10.1016/j.atmosres.2019.104806

Alkhezi AM (2026) A comparative analysis of forecasting models for air temperature: classical time series, machine learning, and functional approaches. Kuwait Journal of Science 53(1):100529. https://doi.org/10.1016/j.kjs.2025.100529

Ateeq-ur-Rauf, Ghumman AR, Ahmad S, Hashmi HN (2018) Performance assessment of artificial neural networks and support vector regression models for stream flow predictions. Environmental Monitoring and Assessment 190(12):704. https://doi.org/10.1007/S10661-018-7012-9

Banerjee A, Gupta S, Priyanshu P, Kar A, Saha R, Chakraborty T, Ghosh D, Kurths J, Hens C (2025) Recent changes in spatiotemporal patterns of heat extremes in South Asia. npj Climate and Atmospheric Science 8:293. https://doi.org/10.1038/s41612-025-01146-1

Beck HE, McVicar TR, Vergopolan N, Berg A, Lutsko NJ, Dufour A, Zeng Z, Jiang X, van Dijk AIJM, Miralles DG (2023) High-resolution (1 km) Köppen-Geiger maps for 1901–2099 based on constrained CMIP6 projections. Scientific Data 10:724. https://doi.org/10.1038/s41597-023-02549-6

Canchala T, Alfonso-Morales W, Carvajal-Escobar Y, Cerón WL, Caicedo-Bravo E (2020) Monthly rainfall anomalies forecasting for southwestern Colombia using artificial neural networks approaches. Water 12(9):2628. https://doi.org/10.3390/w12092628

Chauhan HK, Gallacher D, Bhatt A, Bisht AK (2023) The Himalayas: A climate change laboratory. Environmental Development 45:100814. https://doi.org/10.1016/j.envdev.2023.100814

Che Rose FZ, Rosili NAK, Marsani MF (2025) Comparison of machine learning model performance for predicting the climate variables in Johor Bahru, Malaysia. Scientific Reports 15:23465. https://doi.org/10.1038/s41598-025-08033-y

Cortes C, Vapnik V (1995) Support-vector networks. Machine Learning 20(3):273–297. https://doi.org/10.1007/BF00994018

Elangbam G, Singh AM (2025) How vulnerable are India's North-Eastern hills to climate change? Understanding environmental and socio-economic drivers of climate vulnerability in the state of Manipur. Asia-Pacific Journal of Regional Science 9:265–295. https://doi.org/10.1007/s41685-024-00363-5

Gautam R, Borgohain A, Pathak B, Youroi AS, Kundu SS, Aggarwal SP, Bhuyan PK (2025) Trends and abrupt shifts in mean temperature over North-East India: insights from gridded datasets. International Journal of Environmental Research 19:162. https://doi.org/10.1007/S41742-025-00816-5

Gautam R, Hsu NC, Lau KM, Tsay SC, Kafatos M (2009) Enhanced pre-monsoon warming over the Himalayan-Gangetic region from 1979 to 2007. Geophysical Research Letters 36:L07704. https://doi.org/10.1029/2009GL037641

Getahun YS, Li MH, Pun IF (2021) Trend and change-point detection analyses of rainfall and temperature over the Awash River basin of Ethiopia. Heliyon 7(9):e08024. https://doi.org/10.1016/j.heliyon.2021.e08024

Hamed KH, Rao AR (1998) A modified Mann-Kendall trend test for autocorrelated data. Journal of Hydrology 204(1–4):182–196. https://doi.org/10.1016/S0022-1694(97)00125-X

Hansen JE, Kharecha P, Sato M, Tselioudis G, Kelly J, Bauer SE, Ruedy R, Jeong E, Jin Q, Rignot E, Velicogna I, Schoeberl MR, von Schuckmann K, Amponsem J, Cao J, Keskinen A, Li J, Pokela A (2025) Global warming

has accelerated: are the United Nations and the public well-informed? Environment 67(1):6–44. https://doi.org/10.1080/00139157.2025.2434494

Hawkins E, Williams RG, Young PJ, Berardelli J, Burgess SN, Highwood E, Randel W, Roussenov V, Smith D, Placky BW (2025) Warming stripes spark climate conversations: from the ocean to the stratosphere. Bulletin of the American Meteorological Society 106(5):E964–E970. https://doi.org/10.1175/BAMS-D-24-0212.1

IPCC (2021) Climate change 2021: the physical science basis. In: Masson-Delmotte V, Zhai P, Pirani A, Connors SL, Péan C, Berger S, Caud N, Chen Y, Goldfarb L, Gomis MI, Huang M, Leitzell K, Lonnoy E, Matthews JBR, Maycock TK, Waterfield T, Yelekçi O, Yu R, Zhou B (eds) Working Group I contribution to the sixth assessment report of the Intergovernmental Panel on Climate Change. Cambridge University Press, Cambridge, p 2391. https://doi.org/10.1017/9781009157896

Jain SK, Kumar V, Saharia M (2013) Analysis of rainfall and temperature trends in northeast India. International Journal of Climatology 33:968–978. https://doi.org/10.1002/joc.3483

Jhajharia D, Singh VP (2011) Trends in temperature, diurnal temperature range and sunshine duration in Northeast India. International Journal of Climatology 31(9):1353–1367. https://doi.org/10.1002/JOC.2164

Kendall MG (1975) Rank correlation techniques. Charles Griffin, London

Kent C, Scaife AA, Dunstone NJ, Smith D, Hardiman SC, Dunston T, Watt-Meyer O (2025) Skilful global seasonal predictions from a machine learning weather model trained on reanalysis data. npj Climate and Atmospheric Science 8:314. https://doi.org/10.1038/s41612-025-01198-3

Krishnan R, Sanjay J, Gnanaseelan C, Mujumdar M, Kulkarni A, Chakraborty S (2020) Assessment of climate change over the Indian region: a report of the Ministry of Earth Sciences (MOES), Government of India. Springer, Singapore, p 226. https://doi.org/10.1007/978-981-15-4327-2

Kumar P, Sharma MC, Saini R, Singh GK (2020) Climatic variability at Gangtok and Tadong weather observatories in Sikkim, India, during 1961–2017. Scientific Reports 10:15177. https://doi.org/10.1038/s41598-020-71163-y

Kumar R, Kuttippurath J, Gopikrishnan GS, Kumar P, Varikoden H (2023) Enhanced surface temperature over India during 1980–2020 and future projections: causal links of the drivers and trends. npj Climate and Atmospheric Science 6:164. https://doi.org/10.1038/s41612-023-00494-0

Kumar STP, Lahiri B, Nageswararao MM, Alvarado R, Sangma SN (2023) Trend analysis and changepoint detection of monthly, seasonal and annual climatic parameters in the Garo Hills of Northeast India. Ecological Informatics 75:102104. https://doi.org/10.1016/J.ECOINF.2023.102104

Kumar U, Singh DK, Panday SC, Bisht JK, Kant L (2023) Spatio-temporal trend and change detection of rainfall for Kosi River basin, Uttarakhand using long-term (115 years) gridded data. Arabian Journal of Geosciences 16:173. https://doi.org/10.1007/s12517-023-11244-0

Liu G, Guo Y, Xia H, Liu X, Song H, Yang J, Zhang Y (2024) Increase asymmetric warming rates between daytime and nighttime temperatures over global land during recent decades. Geophysical Research Letters 51:e2024GL112832. https://doi.org/10.1029/2024GL112832

Mann HB (1945) Nonparametric tests against trend. Econometrica 13(3):245–259. https://doi.org/10.2307/1907187

Manzoor S, Ahmad Ahanger M (2022) Spatio-temporal trends in precipitation and temperature means/extremes in the Himalayan states of India. Journal of Water and Climate Change 13(7):2531–2558. https://doi.org/10.2166/wcc.2022.395

Mohammed J, Mengiste Y, Gebremichael M (2025) Enhancing monthly precipitation forecasting by integrating multi-source data with machine learning models: a study in the Upper Blue Nile Basin. Modeling Earth Systems and Environment 11:35. https://doi.org/10.1007/s40808-024-02223-9

Palazzi E, Mortarini L, Terzago S, von Hardenberg J (2018) Elevation-dependent warming in global climate model simulations at high spatial resolution. Climate Dynamics 52:2685–2702. https://doi.org/10.1007/S00382-018-4287-Z

Pandey A, Mondal A, Guha S (2024) Assess the relationship of land surface temperature with nine land surface indices in a northeast Indian city using summer and winter Landsat 8 data. Cogent Engineering 11(1):2382885. https://doi.org/10.1080/23311916.2024.2382885

Parasyris A, Alexandrakis G, Kozyrakis GV, Spanoudaki K, Kampanis NA (2022) Predicting meteorological variables on local level with SARIMA, LSTM and hybrid techniques. Atmosphere 13(6):878. https://doi.org/10.3390/atmos13060878

Paul AR, Maity R (2023) Future projection of climate extremes across contiguous northeast India and Bangladesh. Scientific Reports 13:15616. https://doi.org/10.1038/s41598-023-42360-2

Pepin N, Apple M, Knowles J, Terzago S, Arnone E, Hänchen L, Napoli A, Potter E, Steiner J, Williamson SN, Ahrens B, Dhar T, Dimri AP, Palazzi E, Rameshan A, Salzmann N, Shahgedanova M, Vidal J de D, Zardi D (2025) Elevation-dependent climate change in mountain environments. Nature Reviews Earth & Environment 6:772–788. https://doi.org/10.1038/s43017-025-00740-4

Pepin N, Bradley RS, Diaz HF, Baraer M, Caceres EB, Forsythe N, Fowler H, Greenwood G, Hashmi MZ, Liu XD, Miller JR, Ning L, Ohmura A, Palazzi E, Rangwala I, Schöner W, Severskiy I, Shahgedanova M, Wang MB et al (2015) Elevation-dependent warming in mountain regions of the world. Nature Climate Change 5(5):424–430. https://doi.org/10.1038/NCLIMATE2563

Pettitt AN (1979) A non-parametric approach to the change-point problem. Journal of the Royal Statistical Society: Series C (Applied Statistics) 28(2):126–135. https://doi.org/10.2307/2346729

Rahaman MH, Saha TK, Masroor M, Roshani, Sajjad H (2024) Trend analysis and forecasting of meteorological variables in the lower Thoubal river watershed, India using non-parametrical approach and machine learning models. Modeling Earth Systems and Environment 10:551–577. https://doi.org/10.1007/s40808-023-01799-y

Rahman A, Pekkat S (2025) Multi-model ensemble prediction of maximum and minimum temperature using machine learning approach for North-East India. In: Pandey M, Umamahesh N, Das J, Pu JH (eds) Hydrology and hydrologic modelling. HYDRO 2023. Lecture Notes in Civil Engineering, vol 410. Springer, Singapore. https://doi.org/10.1007/978-981-97-7474-6_14

Rangwala I, Sinsky E, Miller JR (2013) Amplified warming projections for high altitude regions of the northern hemisphere mid-latitudes from CMIP5 models. Environmental Research Letters 8:024040. https://doi.org/10.1088/1748-9326/8/2/024040

Reid PC, Hari RE, Beaugrand G, Livingstone DM, Marty C, Straile D, Barichivich J, Goberville E, Adrian R, Aono Y, Brown R, Foster J, Groisman P, Hélaouët P, Hsu HH, Kirby R, Knight J, Kraberg A, Li J, Lo TT, Myneni RB, North RP, Pounds JA, Sparks T, Stübi R, Tian Y, Wiltshire KH, Xiao D, Zhu Z (2016) Global impacts of the 1980s regime shift. Global Change Biology 22:682–703. https://doi.org/10.1111/gcb.13106

Roshani, Sajjad H, Saha TK, Rahaman MH, Masroor M, Sharma Y, Pal S (2022) Analyzing trend and forecast of rainfall and temperature in Valmiki Tiger Reserve, India, using non-parametric test and random forest machine learning algorithm. Acta Geophysica 71:531–552. https://doi.org/10.1007/S11600-022-00978-2

Roy A, Kolady D, Paudel B, Yumnam A, Mridha N, Chakraborty D, Singh NU (2021) Recent trends and impacts of climate change in North-Eastern region of India-a review. Journal of Environmental Biology 42(6):1415–1424. https://doi.org/10.22438/jeb/42/6/MRN-1701

Saha A, Singh KN, Ray M, Rathod S (2020) A hybrid spatio-temporal modelling: an application to space-time rainfall forecasting. Theoretical and Applied Climatology 142:1271–1282. https://doi.org/10.1007/s00704-020-03374-2

Salaeh N, Ditthakit P, Pinthong S, Hasan MA, Islam S, Mohammadi B, Linh NTT (2022) Long-short term memory technique for monthly rainfall prediction in Thale Sap Songkhla River Basin, Thailand. Symmetry 14(8):1599. https://doi.org/10.3390/sym14081599

Samantaray S, Tripathy O, Sahoo A, Ghose DK (2020) Rainfall forecasting through ANN and SVM in Bolangir Watershed, India. In: Satapathy S, Bhateja V, Mohanty J, Udgata S (eds) Smart intelligent computing and applications. Smart Innovation, Systems and Technologies, vol 159. Springer, Singapore, pp 767–774. https://doi.org/10.1007/978-981-13-9282-5_74

SAPCC (2013) Manipur state action plan on climate change. Directorate of Environment, Government of Manipur. https://moef.gov.in/uploads/2017/08/Manipur1.pdf Accessed 20 July 2025

Satyapragyan S, Yadav JS, Bhambri R (2026) Bias corrections of ERA5 and ERA5-Land temperature using automatic weather station data in the Higher Central Himalaya: implications for hydro-meteorological and glaciological research. Journal of Hydrology: Regional Studies 63:103079. https://doi.org/10.1016/j.ejrh.2025.103079

Sekhri S, Kumar P, Fürst C, Pandey R (2020) Mountain specific multi-hazard risk management framework (MSMRMF): assessment and mitigation of multi-hazard and climate change risk in the Indian Himalayan Region. Ecological Indicators 118:106700. https://doi.org/10.1016/J.ECOLIND.2020.106700

Sen PK (1968) Estimates of the regression coefficient based on Kendall's tau. Journal of the American Statistical Association 63(324):1379–1389. https://doi.org/10.1080/01621459.1968.10480934

Sharma APM, Jhajharia D, Yurembam GS, Srivastava RK (2024) Drought preparedness under changing climate with special reference to Manipur. In: Pathak H, Chatterjee D, Saha S, Das B (eds) Climate change impacts on soil-plant-atmosphere continuum. Advances in Global Change Research, vol 78. Springer, Singapore. https://doi.org/10.1007/978-981-99-7935-6_25

Shrivastava VK, Shrivastava A, Sharma N, Mohanty SN, Pattanaik CR (2023) Deep learning model for temperature prediction: a case study in New Delhi. Journal of Forecasting 42:1445–1460. https://doi.org/10.1002/for.2966

Tamuly G, Deka RL, Goswami B, Goswami J (2019) Trend of temperature regime in the Brahmaputra valley of Assam during 1986–2015. Journal of Agrometeorology 21:106–112.

Tange RI, Rasmussen MA, Taira E, Bro R (2017) Benchmarking support vector regression against partial least squares regression and artificial neural network: effect of sample size on model performance. Journal of Near Infrared Spectroscopy 25(6):381–390. https://doi.org/10.1177/0967033517734945

Vinnarasi R, Dhanya CT, Chakravorty A, Aghakouchak A (2017) Unravelling diurnal asymmetry of surface temperature in different climate zones. Scientific Reports 7:7350. https://doi.org/10.1038/s41598-017-07627-5

Vishal JK, Rani SI (2022) Location-specific verification of near-surface air temperature from IMDAA regional reanalysis. Journal of Earth System Science 131(3):179. https://doi.org/10.1007/s12040-022-01935-9

Vose RS, Easterling DR, Gleason B (2005) Maximum and minimum temperature trends for the globe: an update through 2004. Geophysical Research Letters 32:L23822. https://doi.org/10.1029/2005GL024379

WMO (2025) State of the global climate 2024. WMO-No. 1368. World Meteorological Organization. https://library.wmo.int/idurl/4/69455 Accessed 20 June 2025

Zhong Z, He B, Chen H, Chen D, Zhou T, Dong W, Xiao C, Song X, Guo L, Ding R, Zhang L, Huang L, Yuan W, Hao X, Ji D, Zhao X, Xie SP (2023) Reversed asymmetric warming of sub-diurnal temperature over land during recent decades. Nature Communications 14:7189. https://doi.org/10.1038/s41467-023-43007-6